Geomorphology 295 (2017) 306–322

Contents lists available at ScienceDirect

Geomorphology

journal homepage: www.elsevier.com/locate/geomorph

Late Pleistocene – Holocene surface processes and landscape evolution in the central Swiss Alps

Max Boxleitner[a], Alessandra Musso[a], Jarosław Waroszewski[b], Małgorzata Malkiewicz[c], Max Maisch[a], Dennis Dahms[d], Dagmar Brandová[a], Marcus Christl[e], Raquel de Castro Portes[a], Markus Egli[a,*]

[a] Department of Geography, University of Zurich, Winterthurerstrasse 190, 8057 Zürich, Switzerland
[b] Institute of Soil Sciences and Environmental Protection, Wrocław University of Environmental and Life Sciences, Grunwaldzka 53, 50-357 Wroclaw, Poland
[c] Laboratory of Paleobotany, Department of Stratigraphical Geology, University of Wrocław, Poland
[d] Department of Geography, University of Northern Iowa, Cedar Falls, USA
[e] Laboratory of Ion Beam Physics, ETH Zürich, 8093 Zurich, Switzerland

ARTICLE INFO

Keywords:
Central Alps
Erosion
Mire
Dating

ABSTRACT

The European Alps are a geomorphologically active region and experience a number of gravity-driven hillslope processes. Soil and landscape formation in the Alps has consequently undergone several minor and major traceable changes of developmental trajectories during the Holocene. Soil development is hypothesised to be often non-linear with time and characterised by stages of progressive and regressive evolution caused by up-building (formation, profile deepening) and erosion (profile shallowing). Several cold and warm climate phases are identified during the Holocene but it is largely unknown which effects these might have had on slope processes. By using datable moraines (^{10}Be) and mires (^{14}C), we have constructed a temporal framework for these processes. Using the geochemical imprint of mires in the Alpine setting of the Göschener-valley of the Central Swiss Alps, we reconstructed general (mostly erosional) landscape processes for the last ca. 10 ka. As this is the type locality for the Göschener cold phase, we assumed that this phase (Göschener cold phase I and II ~1.5 and ~2.5 ka BP) should have left easily recognizable traits. After deglaciation (11–12 ka BP), soil evolution was progressive. Beginning around 8 ka BP, we detect a distinct increase in erosion here, together with a vegetation change (towards tundra vegetation) and the highest measured rates of carbon sequestration. Other phases of high geomorphic activity were recognised ca. 5–6 ka BP, 4 ka BP and, to a lesser extent, 1–3 ka ago. The cold phase at 5–6 ka BP corresponds to a less distinct change in vegetation and lessened erosion. Human impact is increasingly obvious since about 2.4 ka BP which overlaps with the Göschener cold phase. Nonetheless, erosion processes were not extraordinarily high during this period and a climate effect cannot be distinguished. We detect evidence of increasing human disturbance (regressive soil evolution) for about the last 1 ka. We also detect an increase in dust flux during the last ca. 4–5 ka, presumably due to the landscape change(s) in the Sahara during this time.

1. Introduction

Deglaciation of the European Alps after the Last Glacial Maximum (LGM) had begun by 21 ka BP (Ivy-Ochs et al., 2006) and ended around the transition to the Holocene. This process was not linear. Although the overall tendency was a general warming with accompanying ice retreat, moraine sequences are preserved in many alpine valleys that witness the climate-driven re-advances or intermittent stable end positions of the Lateglacial. These so-called stadials – primarily to be defined on a local scale before comparing them to regional or even alpine-wide concepts - have been observed and dated in many parts of the Alps.

As a result of the retreating glaciers a vast number of small melt water and kettle lakes — besides the large perialpine lakes (e.g. lake Lucerne) — formed in the Alpine foreland and within the Alps. The concomitant climate warming gave rise to soil-development and re-colonization of the barren landscape by plants. Peatland ecosystems and lake sediments accumulate records of their own developmental history and the surrounding environmental conditions. Due to the processes of erosion and accumulation, sediments filled many of the

* Corresponding author.
E-mail address: markus.egli@geo.uzh.ch (M. Egli).

http://dx.doi.org/10.1016/j.geomorph.2017.07.006
Received 13 May 2017; Received in revised form 29 June 2017; Accepted 4 July 2017
Available online 06 July 2017
0169-555X/

small, newly-formed lakes and mires started to develop (Burga and Perret, 1998; Succow and Joosten, 2001). The soils and mires can, thus, be used as natural archives to decipher landscape evolution and give insight into surface processes in particular and human impact in general (Booth et al., 2005; van der Knaap et al., 2011; Brisset et al., 2013; Jäger et al., 2015; Egli et al., 2015).

Pollen is a trusted proxy for the reconstruction of regional vegetation distribution (Burga and Perret, 1998; Bennett and Willis, 2002; Birks, 2002). Much recent attention has been given to the analysis of pedo- and geochemical signatures in lake sediments and mires that enable us to reconstruct surface processes in their catchment areas (Mourier et al., 2008, 2010; Brisset et al., 2013; Malkiewicz et al., 2016). Using this approach, it has been shown that dominant erosion and soil forming events can be deciphered. A major human impact can be recognised in several parts of the European Alps around 5–6 ka BP (and particularly since 2 ka BP) that has influenced soil mass redistribution (Egli and Poulenard, 2017). In addition, several cold events (or climatic shifts) around 1–3 ka BP (Göschener cold phases I and II: 2.9–2.3 ka BP and 1.6–1.3 ka BP; Zoller et al., 1966; Gamper and Suter, 1982), 4.2, 5–6 ka BP (Piora cold phases) and around 8.2 ka BP (Misox cold phases) are known to have occurred (Haeberli et al., 1999; Magny, 2004; Holzhauser et al., 2005; Joerin et al., 2006; Ivy-Ochs et al., 2009; Berger and Guilaine, 2009; Brisset et al., 2013; Savi et al., 2014). These cold phases are inferred from glacial advances (Haeberli et al., 1999; Holzhauser et al., 2005; Joerin et al., 2006, 2008) and/or changes in timberline (Savi et al., 2014). Ivy-Ochs et al. (2009) summarised glacial advances (of the Lateglacial) based on the ages of erratic boulders on moraines for several glaciers of the central-eastern Alps and climate variations of the Holocene using different proxies. Nicolussi et al. (2005) inferred the existence of warm intervals here by reconstructing the timberline in glaciated valleys.

The Alps are a geomorphologically active region where mass movements on steep slopes take the form of soil erosion, mudflows or debris flows, snow avalanches and solifluction. High mountain valleys experience a number of gravity-driven hillslope processes (Heimsath and McGlynn, 2008) which may depend on climate variations. Soil formation is strongly influenced by hillslope processes. As a consequence, soil development in Alpine areas is often non-linear with time and characterised by phases of progressive and regressive evolution that are due to soil upbuilding (formation, profile deepening) and erosion (profile shallowing) or retardant upbuilding (Johnson and Watson-Stegner, 1987; Sommer et al., 2008; Waroszewski et al., 2016; Zollinger et al., 2017). Facing climatic change, questions about the co-evolution of soils and landscapes arise. Currently, our knowledge in this research field is incomplete and fragmented (e.g. Mavris et al., 2015; Stromsoe et al., 2016).

The main aim of our study is, therefore, to identify changed soil mass-redistribution in the central Alps and, thus, progressive/regressive soil evolutionary steps during the previously mentioned Holocene cold phases — and subsequently also the warm phases in between — by using a geochemical approach. We selected alpine mires as our primary environmental archive. We hypothesised that cold phases in general stimulated erosion phases (and thus regressive soil formation processes). We assumed that, due to lower decomposition rates of organic material, the cold phases gave rise to a higher rate of carbon sequestration in the mires. Because the chosen mires were in the Göschener valley (the type locality of the Göschener cold phases I and II), we assumed that the geochemical and vegetation effects of the cold phases should be fairly obvious here.

2. Materials and methods

2.1. Study area

The study area is located in the Central Alps of Switzerland (Gotthard massif; Fig. 1). This valley has clear evidence of Lateglacial and Holocene glacial activity such as parabolic-shaped surface structures with steep flanks, glacial polish, trimline, whalebacks and other erosional glacial forms. Within the Gotthard region the Göschener-valley is a mainly east–west oriented, approximately 15 km long high alpine valley. It extends from the village of Göschenen (1106 m a.s.l.) at its lower end to the Dammastock (3630 m a.s.l.). The uppermost part of the valley still has glaciers that today are restricted to the valley heads and shady north faces. Distinct moraines formed during the Little Ice Age (LIA) are found in the younger forefields.

The Göschenertal is part of the Aare which comprises biotite-rich coarse-grained granites and syenites. In the upper part of the Chelenalptal and the Voralptal (side valleys) a variety of different crystalline rocks are found, including the light-coloured middle-grained Voralpgranite, migmatites, mica shists, gneiss and amphibolite (Labhart, 1992).

Two subsites were investigated in the Göschener-valley (Fig. 1). The ‘Brätschenflue’ area is located north of the Göscheneralpsee (Fig. 2) and is one of the most notable whaleback/roche moutonnée bands in Switzerland. After glacial retreat, several mires and small ponds developed between the glacially polished granite bedrock backs. The peat cores at ‘Brätschenflue’ were retrieved from the thickest mire deposits. A prominent 1.7 km long lateral moraine is located 120 m above and to the north of the mire. From here we took rock samples from moraine boulders (Bergstaffel 1 and 2) for surface exposure dating. The second sampling site (‘Börtli’) is located ca. 1.5 km downvalley on a further extension of this moraine (Fig. 3). At ‘Börtli’, the moraine is well discernible over a length of approximately 450 m. Small remnants of another former ice margin can be identified about 70 m to the north, parallel to the moraine's footslope. The larger moraine here served as a natural barrier and sediment trap. Today the area between the moraines is occupied by the ‘Börtli’ peat bog that is up to 3 m deep. The lateral moraines that enclose the Brätschenflue and the Börtli sites can be traced on both sides of the Göschener valley. To further constrain the age of this moraine complex we took rock samples for surface exposure dating on its left lateral, behind the Voralp tributary at the ‘Golderen’ site (Fig. 3) and on the right lateral at the ‘Börtlistafel’ site.

2.2. Sampling strategy and procedure

We took two core drillings at each of the Börtli and Brätschenflue sites. The Börtli site (A, B) is located at 1805 m a.s.l. at the toeslope (in the adjacent northern part) and delimited to the south by a pronounced Lateglacial lateral moraine. The Brätschenflue site (BF A, B) is at 1910 m a.s.l. and about 2 km west of the Börtli site. This mire is embedded in a glacially polished landscape with numerous, almost perfectly shaped ‘roches moutonneés’ (Aare granite). From a geomorphic point of view, the Börtli site better reflects slope processes than the BF site, due to its close proximity to steep slopes. The BF site should more accurately reflect aeolian additions as it is less masked by slope related inputs into the mire. At both sites, we chose the best position for drilling by use of an avalanche probe to detect the thickest and, presumably, oldest layers in the mire. Cores were drilled to the inorganic sediment layer or bedrock. In addition, we sampled two soil profiles on the backslope close to the Börtli mire (Table 1). Profiles were dug to the parent material where possible and 1–2 kg of soil material per horizon were taken for the chemical and physical analyses (after Hitz et al., 2002).

Moraines, as traces of glacial advances, represent the maximum downvalley extent of a glacier at a certain point in time. The age of moraine-formation can be directly addressed and related to other independent archives by the use of surface-exposure-dating. We took five rock samples from moraine boulders here. We chose large, flat-topped boulders to avoid edge effects (Masarik and Wieler, 2003) protruding > 1 m from the surrounding sediments. The position (latitude/longitude and altitude) of the sample sites was recorded with GPS and verified with topographic maps. The geometry of a boulder and the

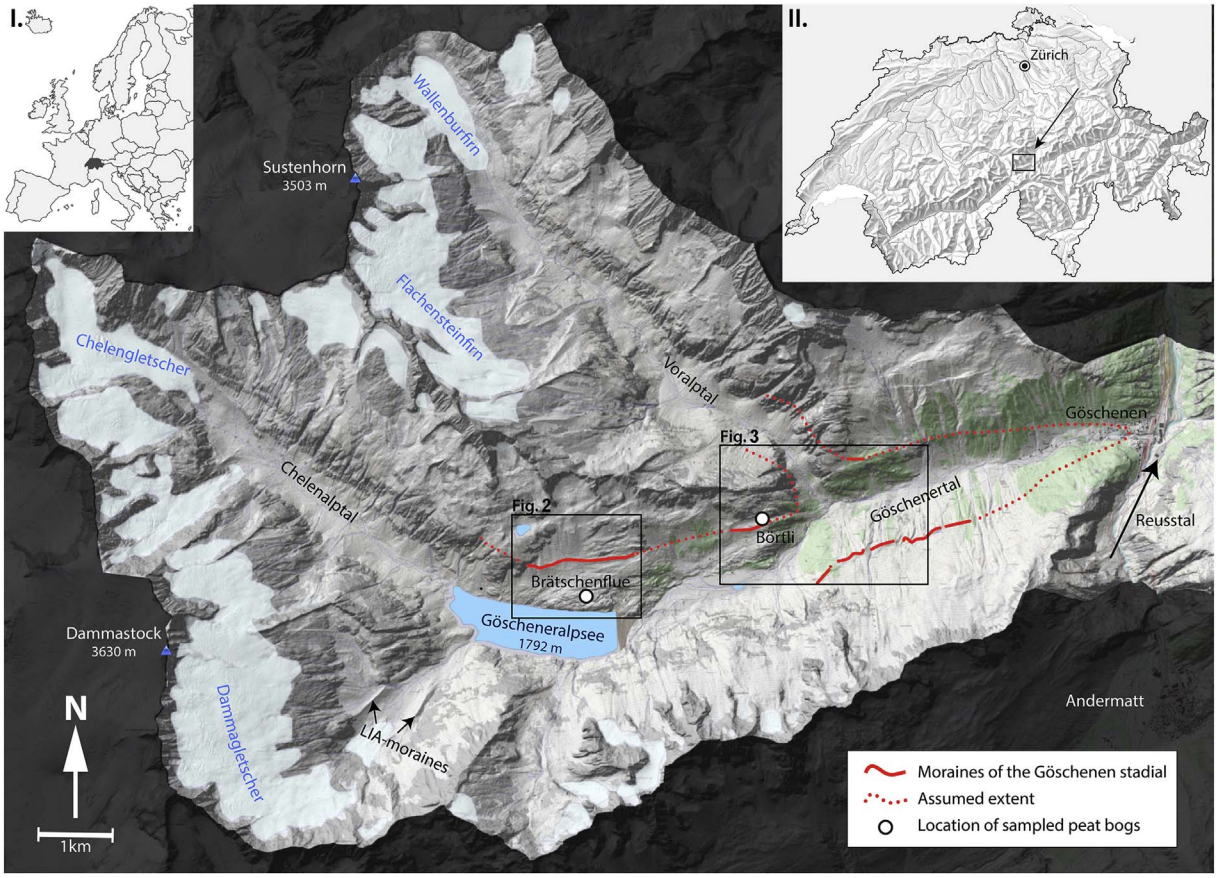

Fig. 1. General overview of the investigation area Göschener-valley with tributaries. Reproduced by permission of swisstopo (BA17068)

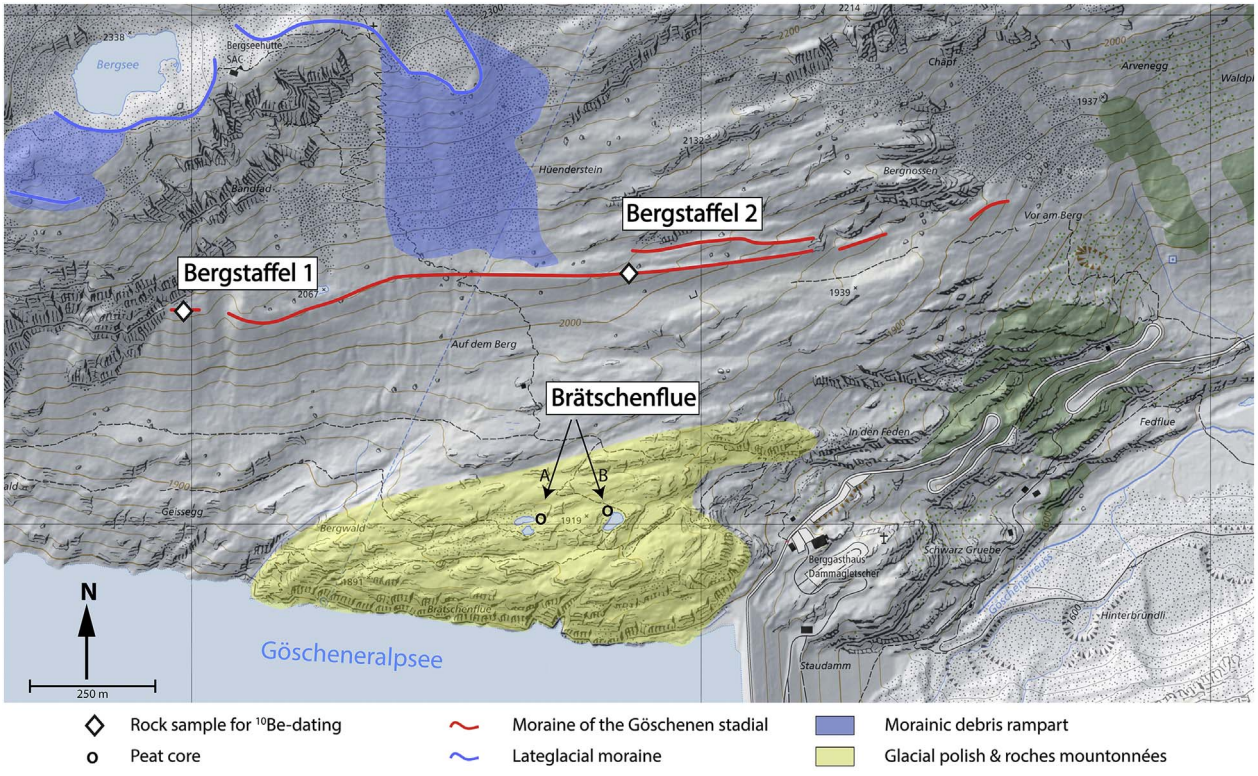

Fig. 2. Subsite Brätschenflue with location of mire core drillings and moraine sampling locations. Reproduced by permission of swisstopo (BA17068)

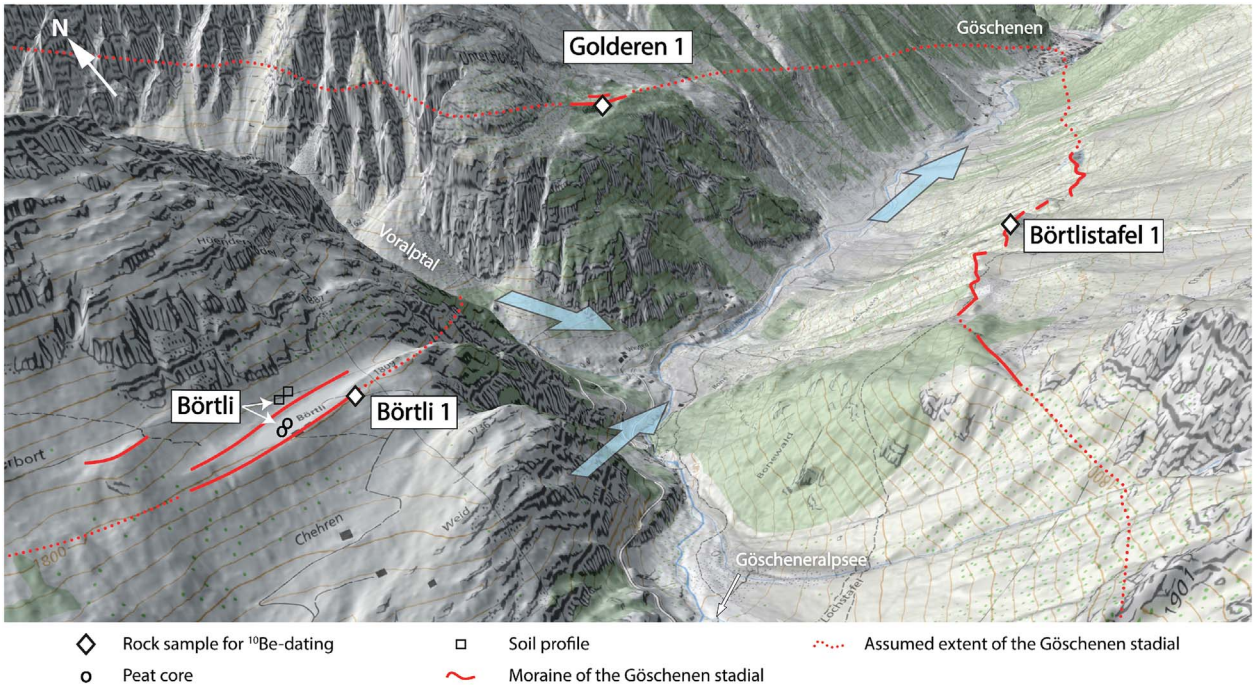

Fig. 3. Subsite Börtli with location of mire core drillings, soil and moraine sampling locations. The blue arrows indicate the ice flow direction of the former glaciers. Reproduced by permission of swisstopo (BA17068). (For interpretation of the references to colour in this figure legend, the reader is referred to the web version of this article.)

effect of topographic shielding by surrounding mountains both have an influence on the amount of cosmic radiation. To correct for these important effects we measured the dip of the rock surface, the direction of the dip and the shielding effect. Because cosmic rays are distinctly attenuated within the rock material, production of cosmogenic isotopes is highest directly at the surface. We therefore sampled the uppermost centimetres of the rock surface and documented the sample thickness.

2.3. Chemical and physical analyses of the mires and soils

The bulk density of the soil and mire material was measured on undisturbed samples (volumetric sampling). Oven-dried samples (70 °C; 48 h) were sieved to < 2 mm (fine earth) and homogenised. After a pretreatment of the soil samples with H_2O_2 (3%), particle-size distribution of the fine-earth was measured using a combined method consisting of wet-sieving the coarser particles (2000–32 μm) and determining the finer particles (< 32 μm) by means of an X-ray sedimentometer (SediGraph 5100). Soil pH (0.01 M $CaCl_2$) was determined using a soil:solution ratio of 1:2.5 and a peat:solution ratio of 1:12.5. Loss on ignition (LOI) was measured for 110 samples on the 2.0 g oven-dried - milled fine earth fraction (< 63 μm), ignited at 550 °C for 5.5 h. Organic C and N contents (determined in duplicate) were measured using a C/H/N analyser (Leco). The standard reference material is EDTA (Säntis Analytical, article no SA502092) having C = 41.09%, H = 5.52%, *N* = 9.58%, O = 43.8% (measured values were C: 41.11 ± 0.08%; H: 5.53 ± 0.08%; N: 9.57 ± 0.08%, O: 43.79 ± 0.08). Total elemental content was determined by X-ray fluorescence after the soil and peat material was milled to < 63 μm in a tungsten carbide horizontal mill (Retsch®, Germany). Powder samples (in duplicate) of approximately 5 g material were analysed with an energy dispersive He-flushed X-ray fluorescence spectrometer (ED-XRF, SPECTRO X-LAB 2000, SPECTRO Analytical Instruments, Germany). The quality of the analyses was checked using a soil reference material (Reference Soil Sample CCRMP SO-4, Canada Centre for Mineral and Energy Technology) with certified total element concentrations.

2.4. Mineralogy

We used DRIFT (Diffuse Reflectance Infrared Fourier Transform spectroscopy) to qualitatively describe mineralogical properties of the soils and mires. An overview of the minerals present in the < 2 mm fraction was obtained by recording DRIFT-spectra (Bruker, Tensor 27) from 4000 to 250 cm^{-1} using a powder containing 30 mg of sample (10% of the total weight) and 270 mg KBr (90% of the total weight). Prior to measurement, the samples were again oven-dried at 80 °C. The FT-IR spectra were interpreted using the OPUS 6.5 software. Quartz was recognised by the typical peak doublet at 780 and 800 cm^{-1}. The peaks at 3694 and 3622 cm^{-1} are attributed to kaolinite, those at 3624 and 531 cm^{-1} to mica, those at 375 and 346 to imogolite type material (ITM) and those at 3620, 3526, 3469 and 1017 cm^{-1} to gibbsite (Farmer et al., 1978; Egli et al., 2008; Jäger et al., 2015).

2.5. Calculation of stocks and carbon sequestration rates in the mires

Carbon stocks were calculated for the mire and for individual depth ranges according to the following equations:

Table 1
General characteristics of the investigated soils.

Site	Coordinates	Vegetation	Elevation (m a.s.l.)	Slope (°)	Exposure (°N)	Soil type WRB (IUSS Working Group, 2015)
Soil 1	46°39′29″ N/8°31′13″E	Alpine grassland	1817	42	175	A-horizon overlying an eroded (Entic or Albic) Podzol
Soil 2	46°39′29″ N/8°31′11″E	Alpine grassland	1828	42	170	A-horizon overlying an eroded (Entic or Albic) Podzol

Table 2
Sample properties. Latitude and longitude are in WGS84 coordinates. Shielding correction includes the effects caused by mountain topography, dip and strike of the various boulder surfaces. Rock density is 2.7 g/cm^3 throughout.

Nr.	Sample name	Latitude	Longitude	Elevation	Thickness	Shielding factor	Quartz	Carrier	^{10}Be content	Uncertainty ^{10}Be content	Exposure age	Internal uncertainty
		(DD)	(DD)	(m a.s.l)	(cm)		(g)	(mg)	(atoms g^{-1})	(atoms g^{-1})	(a)	(± a)
1	Bergstaffel 1	46.653	8.484	2091	3	0.918	30.53	0.350	2.26E + 05	9.01E + 03	11,414	460
2	Bergstaffel 2	46.654	8.495	2034	3	0.977	30.65	0.353	2.47E + 05	8.51E + 03	12,202	426
3	Börtli A	46.658	8.522	1803	6	0.956	31.34	0.341	1.57E + 05	8.78E + 03	9594	542
4	Golderen 1	46.665	8.540	1746	3	0.952	31.08	0.351	2.06E + 05	7.13E + 03	12,904	453
5	Börtlistafel 1	46.655	8.544	1649	2	0.966	31.53	0.351	1.81E + 05	7.09E + 03	11,887	472

$$C_{stock} = \sum_{i}^{dz} c_i \rho_i d_i \text{ for the profile and } C_{stock,d_i} = c_i \rho_i d_i \text{ for a specific depth range} \quad (1)$$

C_{stock} denotes the carbon stocks over the indicated soil depth (kg m^{-2}), c the organic carbon concentration (kg t^{-1}), ρ the bulk density (t m^{-3}) and d the thickness of the considered layers.

We calculated the time necessary to build up peat for a given layer thickness using an age-depth model (see below). Dividing the stocks of a specific depth range by the corresponding time resulted in the sequestration rate (g C m^{-2} a^{-1}).

2.6. Weathering indices

Various chemical weathering indices have been developed to trace element leaching and weathering (Parker, 1970; Kronberg and Nesbitt, 1981; Buggle et al., 2011; Schatz et al., 2015). A common feature of these indices is that easily leachable elements such as Ca, Mg, K and/or Na are compared to less weatherable and transferable elements such as Al, Fe, Si, Ti etc. Most of the indices refer to the chemical weathering of silicates. Depending on the mathematical procedure, either an enrichment of 'immobile' elements or a depletion of the mobile base cations are calculated.

Index B is defined by the molar ratio of:

$$B = \frac{CaO + K_2O + Na_2O}{Al_2O_3 + CaO + K_2O + Na_2O} \quad (2)$$

The CIA (chemical index of alteration) is defined as:

$$CIA = 100\left[\frac{Al_2O_3}{Al_2O_3 + CaO + Na_2O + K_2O}\right] \quad (3)$$

As Ti is considered to be an immobile element (Dahms et al., 2012), the (K + Ca)/Ti ratio can be used as additional weathering index: the lower the ratio, the higher the degree of weathering.

2.7. Pollen analysis

Profile sequences for three mire cores from Börtli and Brätschenflue were analysed for their pollen spectra. Organic (peat) samples were heated in a 10% KOH solution to remove the humified organic matter; the mineral samples were treated using 40% HF to dissolve siliceous minerals (Faegri and Iversen, 1989). Thereafter, cellulose was destroyed using acetolysis (Erdtman, 1960). 400–1000 sporomorphs were counted in each sample on 2–4 glass slides. Pollen grains were detected in both profile sequences in a sufficient amount, except at the Börtli site at a depth of 120–150 cm. Calculations of the pollen spectra were done for both cores (except Börtli, 120–150 cm depth). We determined the percentage of arboreal (tree species) and non-arboreal (shrubs and herbaceous species) pollen based on the abundance of individual species or groups of taxa. Cryptogams were constructed for the Brätschenflue site. The palynological software POLPAL was used to plot the pollen diagrams (Nalepka and Walanus, 2003).

2.8. Surface exposure dating (^{10}Be)

The rock samples were pre-treated following the procedures of Kohl and Nishiizumi (1992) and Ivy-Ochs (1996). Samples were crushed and sieved and the quartz isolated by treating the 0.25 mm–0.6 mm fraction with *aqua regia* to destroy organic contaminations and any calcareous components. After a 1 h–treatment with 0.4% HF, we used a floatation system to physically separate feldspar and mica components from quartz. Remaining remnants of these were removed by repeated 4%HF leaching steps. Once pure quartz was obtained, we added a ^{9}Be-carrier solution and dissolved the samples in 40%HF. Be was isolated using anion and cation exchange columns followed by selective pH precipitation techniques (von Blanckenburg et al., 1996). The Be hydroxides were precipitated, dried, and calcinated to BeO at 850 °C. The ^{10}Be/^{9}Be ratios were measured at the ETH Laboratory of Ion Beam Physics' Accelerator Mass Spectrometry (AMS) facility using the ^{10}Be standard S2007 N with a nominal value of ^{10}Be/^{9}Be = 28.1 × 10^{-12} (Christl et al., 2013; Kubik and Christl, 2010). S2007 N has been calibrated to the ^{10}Be standard ICN 01-5-1 of K. Nishiizumi and has a nominal ^{10}Be/^{9}Be value of 2.709 × 10^{-11}(Nishiizumi et al., 2007). The 1σ error of S2007 N is 2.7% (Christl et al., 2013). Measured ^{10}Be/^{9}Be ratios were corrected for ^{10}Be contributed by the Be-carrier (blank value: 0.003E-12). ^{10}Be concentrations and according one sigma uncertainties are reported in Table 2.^{10}Be exposure ages were calculated using CRONUS-Earth (http://hess.ess.washington.edu/math/) version 2.3 with a ^{10}Be production rate of 4.01 ^{10}Be atoms/g SiO_2/year (Borchers et al., 2016) and a ^{10}Be half-life of 1.387 ± 0.012 Ma (Chmeleff et al., 2010; Korschinek et al., 2010). The production rate was corrected for latitude and altitude using the scaling scheme of Stone (2000) and corrected for sample thickness assuming an exponential depth profile (Brown et al., 1992) with an effective radiation attenuation length of 160 g cm^{-2} (Gosse and Phillips, 2001) and a rock density of 2.7 g cm^{-3}. We assumed a rock erosion rate of 1 mm/ka and but applied no correction for snow. Effects of variations of the geomagnetic field on the ^{10}Be age are said to be negligible (Masarik et al., 2001; Pigati and Lifton, 2004).

2.9. Radiocarbon dating

Peat and wood samples were cleaned using an acid-alkali-acid (AAA) treatment. The samples (cleaned charcoal, peat and wood samples and soil sample fractions) were heated under vacuum in quartz tubes with CuO (oxygen source) to remove any absorbed CO_2 in the CuO. The tubes were then evacuated again, sealed and heated in the oven at 900 °C to obtain CO_2. The CO_2 of the combusted sample was mixed with H_2 (1:2.5) and catalytically reduced over iron powder at 535 °C to elemental carbon (graphite). After reduction, the mixture is pressed into a target and carbon ratios were measured by Accelerator Mass Spectrometry (AMS) using 0.2 MV radiocarbon dating facility (MICADAS) of the Ion Beam Physics at the Swiss Federal Institute of Technology Zurich (ETHZ). The calendar ages were obtained using the OxCal 4.2 calibration program (Bronk Ramsey, 2001, 2009) based on

the IntCal 13 calibration curve (Reimer et al., 2013). Calibrated ages are given in the 2σ range (minimum and maximum value for each). Age-depth modelling was performed using the R-code 'clam' (Blaauw, 2010). When 14-C ages are reported, then the age indication is given in cal (k)a BP. More general age indications (not or not purely related to ^{14}C) are given as (k)a BP).

3. Results

3.1. Timing of the geomorphic settings

As all dated rock samples are from the same moraine complex, our exposure ages between 11.4 and 12.9 ka (Table 2) indicate that the entire Göschenertal was covered by ice during the Younger Dryas (Blockley et al., 2012; Rasmussen et al., 2014). The ca. 9.6 ka age of boulder Börtli A appears to be anomalously young. Although we did not find an obvious indication in the field, the boulder could have toppled, its surface spalled or exhumed from the moraine after deposition. One of these processes could explain the younger-than-expected age of this boulder.

An additional, indirect way to assess glacier retreat is to date the transition layer from glacial sediments to organic deposits of a peat bog, to provide a minimum-limiting age for the disappearance of the glacier from the area. The Börtli mire (Fig. 3) developed directly outside of the border of the Younger Dryas moraine and is, therefore, morphostratigraphically connected directly to this landform. The Brätschenflue mire could likewise only develop after ice retreated from its Younger Dryas position here.

3.2. Soils

The soils sampled at the Börtli site developed on the moraine deposits and colluvial hillslope material, both with granitic characteristics. The soils exhibit two parts – an eroded soil and on top a younger A horizon giving rise to Ah1-Ah2-2Bsb/BCb profiles. The soils contain a considerable amount of gravel (Table 3). The highest gravel content was measured in the 2Bsb and 2BCb horizons. The silt and clay contents decrease from the surfaces (loam) to the 2BCb horizons (sandy loams). Bulk densities increase from the A horizons (< 1 g cm^{-3}) to the 2BCb horizons (~ 1.3 g cm^{-3}). The lowest pH-values were measured in the Ah horizons and increased with depth. Both soils have organic-rich topsoils with org. C values from 17 to 20% (Table 3). Organic matter was present in significant amounts (2–3%) to depths of > 60 cm. Similarly, the LOI showed very high values in the topsoils and strongly decreased with depth in the subsoil. C/N ratios were rather uniform along the profile and varied from 14-to-19.

The SiO_2 contents are high in these soils, typically for soils with granitic compositions (Table 4). We expect generally to see the Si content increase with depth in soils such as these due to the 'dilution effect' of high amounts of organic matter in the topsoils. Moderately comparable trends with depth also were detected for all cations but Ca, Mn and P, where the highest concentrations were found in the topsoil.

Because soil weathering proceeds from the surface towards depth, the most intensively weathered material should be found near the soil surface. On stable surfaces, where a progressive evolution takes place, the lowest (K + Ca)/Ti ratio has be expected in the topsoil. This is clearly not the case for our soils (Table 4). The B-index and the CIA of these soils also occur contrary to our expectations. It appears that the topsoils are less weathered than the subsoils or have slightly different chemical compositions. Most likely, materials with slightly different granitic compositions were eroded from upslope positions and deposited here on a previously truncated soil profile.

The DRIFT analyses of the soil material reflect the granitic composition. Typical minerals are quartz and mica (muscovite; Table 5). Kaolinite is detected in the topsoil but not in the 2BCb and 2Bsb2 horizons. Traces of ITM mainly appear in the 2Bsb horizons. Traces of gibbsite (a product of silicate weathering) was detected in the topsoils and at higher abundance in the subsoils.

3.3. Mire cores

The mire cores Börtli A and B were taken relatively close to each other (10–15 m) and show similar depth trends for bulk density and pH (Fig. 4). Bulk density decreased in the first 50–100 cm, from 0.2 to 0.1 g cm^{-3}. The higher densities close to the surface are most likely due to the management of the site (drainage; partially used as pasture). The Börtli A core shows little variation with only one significant change at 200 cm due to a layer of inorganic material mixed into the peat. The Börtli B core shows the same increase at 200 cm, but also shows distinct peaks at 90 and 130 cm. At the peat base, the bulk density also increased. Both profiles are acidic with pH values in the range of 3.3 to 4. A slight increase in pH towards the peat base and towards to the surface was measured.

Organic matter content (LOI) is nearly 100% throughout the profiles. The organic C (30–55%) trend with depth (data not shown) is nearly identical to LOI (Fig. 5). The SiO_2 content varies only slightly along the Börtli A core whereas core B shows distinct peaks at 125 to 135 cm, at 205 cm and at 278 cm (Fig. 5). These peaks match the sediment layers found in the peat at the same levels. Al_2O_3 follows the same trends, which is expected, since Al and Si represent the input of silicates into the mires. The TiO_2 and ZrO_2 contents mirror the patterns of SiO_2 and Al_2O_3.

The major minerals found in the soils surrounding the mires were also detected in the mire sediments (Table 5). Consequently, a large part of the sediment input apparently derives from a local source. It is, however, interesting to note that Kaolinite appears mainly in the uppermost metre of the mires.

The Brätschenflue mires are located at a higher altitude (above the present-day timberline) than the Börtli site. Unlike at Börtli, the Brätschenflue cores (BF A and BF B) were at different bogs (aerial

Table 3
Physical and some main chemical characteristics of the investigated soils.

Profile	Horizon	Depth	Munsell colour	Bulk density	Sand	Silt	Clay	Gravel[a]	pH	C	N	C/N
		cm	(moist)	(g/cm^3)	w.-%	w.-%	w.-%	w.-%	($CaCl_2$)	g/kg	g/kg	
Soil 1	Ah1	0–5	10YR 2/2	0.52	39.1	36.0	25.0	10	4.54	200.4	11.6	17.3
	Ah2	5–15	10YR 2/2	0.81	42.8	39.7	17.6	45	3.80	108.0	6.5	16.5
	2Bsb	15–60	10YR 3/4	0.88	57.3	36.6	6.2	32	4.16	39.9	2.5	16.2
	2BCb	> 60	10YR 3/4	1.23	71.3	24.6	4.1	55	4.50	31.2	1.6	19.2
Soil 2	Ah1	0–5	10YR 2/1	0.70	47.3	34.4	18.3	28	3.95	169.7	11.7	14.5
	Ah2	5–18	10YR 2/2	0.86	51.7	32.4	15.9	25	3.68	79.2	5.8	13.6
	2Bsb1	18–60	10YR 3/3	0.88	50.6	37.8	11.7	45	3.90	29.0	1.8	16.4
	2Bsb2	> 60	10YR 3/4	1.28	62.7	33.1	4.2	56	4.13	21.6	1.2	18.6

[a] Fraction > 2 mm.

Table 4
Total elemental contents (in oxide form) and chemical weathering indices (molar ratios).

Profile	Horizon	Na_2O	MgO	Al_2O_3	SO_3	SiO_2	P_2O_5	K_2O	CaO	TiO_2	MnO	Fe_2O_3	LOI	(K + Ca)/Ti	B-index	CIA
		g/kg	g/kg	g/kg	g/kg	g/kg	g/kg	g/kg	g/kg	g/kg	g/kg	g/kg	g/kg			
Soil 1	Ah1	26.0	16.3	101.6	3.65	450.2	2.51	22.30	12.21	7.50	1.93	45.3	310.5	7.36	0.47	0.53
	Ah2	29.8	15.6	126.6	2.25	569.1	1.63	27.47	9.25	8.27	1.16	47.8	161.1	7.23	0.43	0.57
	2Bsb	29.3	20.6	150.2	1.67	594.5	2.28	30.99	9.56	10.49	1.98	64.1	84.3	6.31	0.40	0.60
	2 BCb	28.2	32.0	170.5	1.63	573.4	1.70	31.13	9.00	9.90	0.97	75.3	66.4	6.63	0.36	0.64
Soil 2	Ah1	32.3	11.6	111.3	3.45	559.5	2.34	30.48	9.38	5.16	1.29	28.9	204.2	12.62	0.48	0.52
	Ah2	32.8	10.0	121.6	2.08	637.0	1.61	33.21	8.35	5.47	0.80	29.0	118.1	12.47	0.46	0.54
	2Bsb1	34.9	11.7	137.4	1.06	668.5	1.48	35.42	9.60	7.65	0.52	36.8	54.9	9.64	0.45	0.55
	2Bsb2	32.9	24.7	156.3	1.10	614.1	1.36	34.55	9.07	8.65	1.11	64.8	51.4	8.27	0.41	0.59

Table 5
Detected main minerals in the mires (Börtli A and BF A) and the soil profiles using DRIFT. x = present, (x) = minor amount.

	Depth/horizon (cm)	Kaolinite	Gibbsite	ITM[a]	Quartz	Mica
Börtli A	5	x	x		x	(x)
	25	x	x			
	45	x	(x)	(x)		
	65	x		x	(x)	
	85	x	x	(x)	(x)	
	105		x		x	(x)
	125	(x)	(x)	(x)	(x)	(x)
	150			(x)	(x)	(x)
	165		(x)	(x)	(x)	
	185	(x)	(x)	x	(x)	
	205		x	(x)	(x)	(x)
	230	(x)		(x)	(x)	
	250			x		
	270			(x)		
	290				(x)	(x)
BF A	20	x	(x)	(x)	x	(x)
	30	(x)		(x)	(x)	x
	50	x	(x)	x	x	x
	70	(x)	(x)	x	x	x
	90	x	(x)	x	x	x
	105	x	(x)	(x)	x	x
	115	(x)			(x)	x
	125	x	(x)	x	x	x
	135	(x)		(x)	x	x
	150	x	(x)	(x)	x	(x)
	165	(x)		x	x	x
	175			(x)	x	(x)
	190		(x)		x	(x)
	210		(x)		(x)	(x)
	225		x		(x)	(x)
	235			(x)	x	(x)
	250	(x)	(x)			
	265	(x)		(x)	x	(x)
	275	(x)			x	(x)
	285	(x)	x	(x)	x	(x)
	295	(x)	x	(x)	x	x
Soil 1	Ah		(x)	x	(x)	x
	AE	x	(x)		x	x
	2Bs	x	x	x	x	x
	2BC		x		x	x
Soil 2	Ah	x	(x)	(x)	x	(x)
	AE	x	x		x	(x)
	2Bs1	x	x	(x)	x	x
	2Bs2		(x)		x	x

[a] ITM = Imogolite-type material, henceforth referred to as the sum of imogolite and proto-imogolite allophane.

distance was roughly 100 m). The maximum depth was 300 cm for the BF A core and 220 cm for core BF B. With a thinner coring device, we retrieved organic remnants from 290 cm at the site BF B. The dry bulk density is very low in both cores, especially in BF A where a value above 0.1 g cm^{-3} was rarely reached (Fig. 4). Both mires do not show a present-day human impact because they are under legal protection. Nonetheless, some visible traces of former human activity can be seen in this area in the form of former turf mining). The mire profiles have pH values between 3.2 and 4.2, with a tendency to increase pH with depth. The depth trends of LOI and organic C (data not shown) are congruent. The BF A and B profiles are characterised by a very high LOI (with values up to almost 100%) over large parts of the profiles. In profile BF A, we measured SiO_2 and Al_2O_3 peaks at 50, 125, 160 and below 250 cm. The increase in SiO_2 and Al_2O_3 at 250 cm depth is due to the transition of peat to the sediment base. The TiO_2 and ZrO_2 contents reflect the same depth-trends. Similar to the Börtli site, the minerals detected at Brätschenflue reflect a granitic composition (quartz, mica). Kaolinite occurs in higher concentrations in the upper part (i.e., 0–150 cm).

3.4. Radiocarbon dating

A total of 15 samples was dated for this study (Table 6) with a maximum age of ca. 9 ka cal BP). The full sequence for the Börtli and Brätschenflue sites is shown in Table 6 and Fig. 6. The Börtli profile shows a slight age inversion at its base. According to the modelled age trend (Fig. 6), a linear continuation with depth would have been expected (Fig. 6; speculated trend given as a dashed orange line). The Börtli mire is probably slightly older than Brätschenflue. At Brätschenflue, peat formation started about 8.5 ka cal BP (both profiles BF A and BF B indicate the same result) whereas the onset of peat formation at the Börtli site may have started as early as 10 ka cal BP. The area where the mires are found was, however, ice-free earlier. Following ice melt, it may take several centuries up 1–3 ka until a mire starts to form (e.g. Madole, 1976).

3.5. Pollen analysis

3.5.1. Börtli

The most dominant tree pollen are *Alnus* and *Picea abies*, and to a lesser extent *Corylus avellana, Quercus, Ulmus, Abies alba* and *Fagus sylvatica* (Fig. 7). The most abundant families and species are Cyperaceae, Poaceae, Apiaceae, Ateraceae and Filicales monoletae. The arboreal to non–arboreal pollen (AP:NAP) ratio is 80–90:10 and fairly stable, showing only one broad peak in non–arboreal pollen between 170 and 220 cm (ca. 7.9–8.7 cal ka BP; Fig. 7). The lower part of the core (230–285 cm) corresponds to an age of ca. 8.8–9.7 cal ka BP) and is dominated by *Betula* (30–48%) with a minor share of *Picea abies* (c. 17%). No pollen was detected between 120 and 150 cm. *Betula* is very abundant below this zone (≥ 6.5 ka BP) and strongly reduced above it (≤ 5.6 ka BP). A similar pattern is detected for Cyperacea (Populus). In contrast, more *Fagus sylvatica* or *Carpinus betulus* pollens are present after 5.6 ka BP. The trends of *Alnus* and *Picea abies* and the differences in pollen distribution patterns above and below this gap indicate the existence of an abrupt climatic shift here during this period.

The proportion of *Betula* strongly decreases above the gap (after 5.6 ka BP). *Alnus* (40%) and *Picea abies* (up to 45%) now dominate the spectra. A very minor proportion of *Salix* appears at 65 cm (about

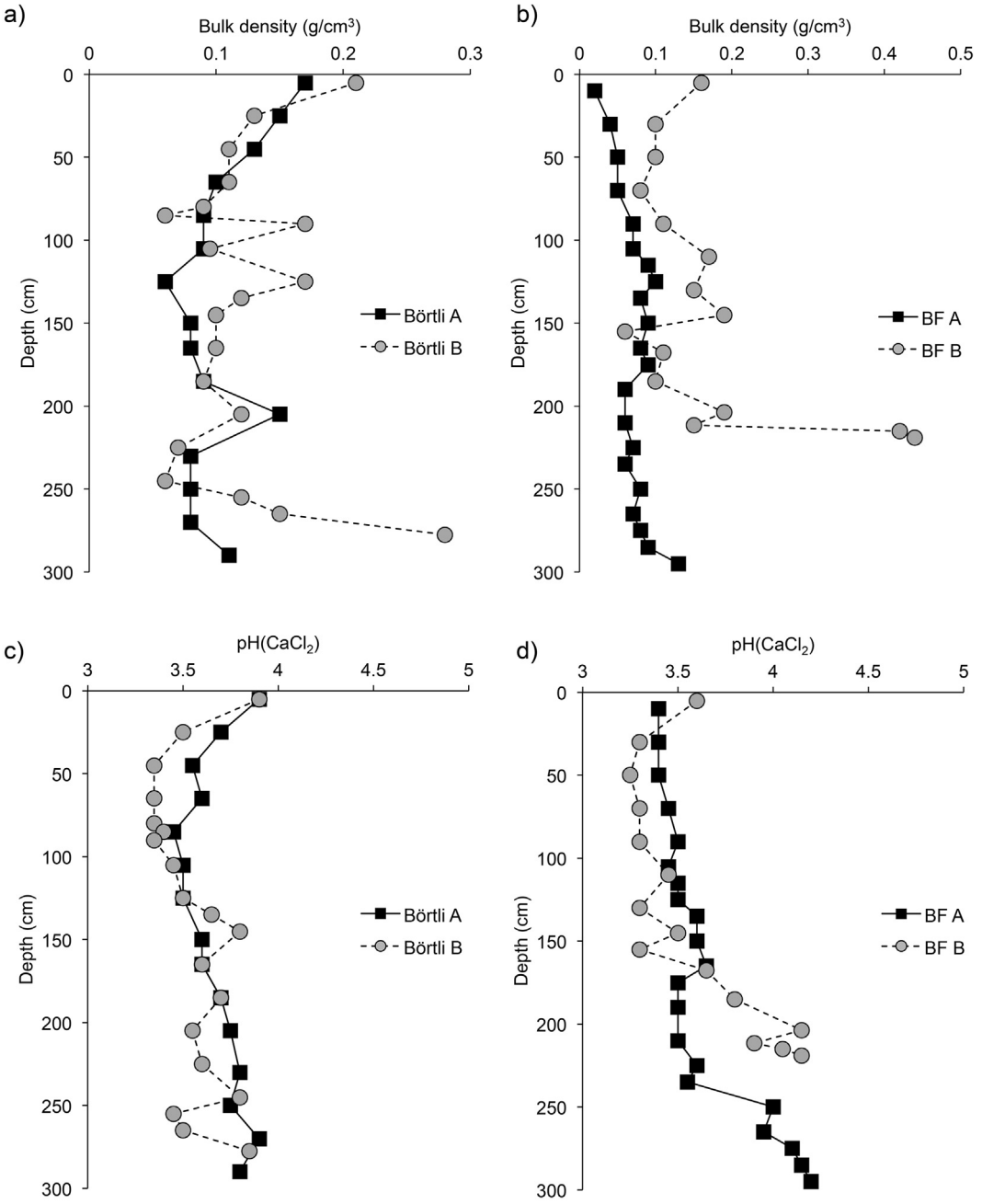

Fig. 4. Bulk density for a) Börtli and b) BF (Brätschenflue) and pH-value as a function of depth for c) Börtli and d) BF.

2.7 cal ka BP) suggesting slightly more humid conditions are present at this time. The presence of *Fagus* and *Carpinus* indicate temperatures also are warmer, but then their proportions decrease after 2900 cal BP. Typically human–related species, such as Brassicaceae, *Plantago lanceolata*, Calluna and Galium increasingly appear at ca. 30–55 cm (1.1–2.4 cal ka BP).

3.5.2. Brätschenflue

The pollen analysis yielded more data for trees and shrubs, but little for herbs. The highest content of pollen comes from tree species such as *Picea abies*, *Corylus avellana*, *Ulnus*, *Abies alba*, and to a lesser extent from *Quercus* and *Populus*. The small amounts of herb pollen mostly consist of Cyperaceae and Poaceae. The AP:NAP ratio varies around 80–90:10 with slight variations. A slightly higher proportion of NAP was measured at 170–185 cm (corresponding to ca. 3.6–4.1 cal ka BP), 100–110 cm (ca. 1.6–1.9 cal ka BP), 70–80 cm (ca. 1.0–1.2 cal ka BP) and from 40 to 50 cm (ca. 500–700 cal a BP) on to the surface. The variations in the AP:NAP ratio strongly correlate with the relative proportion of *Pinus sylvestris* pollens from the surface to ca. 200 cm. Below 200 cm, *Betula* is present at a much higher proportion and the AP:NAP ratio is more governed by birch.

According to the pollen distribution, the Brätschenflue core can be subdivided into four main phases:

- Phase I (220–170 cm; 3.6 to 5.4 cal ka BP) has a high share of *Corylus* (20–35%) together with *Betula* (18–28%), *Pinus* (9–14), *Ulmus* (8%), *Alnus* (4–12%), *Quercus* (3%) and *Tilia* (2–3%). These species indicate the presence of mixed forests at this time that were not very dense and had an open structure (due to the presence of Calluna, Poaceae). *Salix* and *Huperzia selagdo* indicate semi–cold, humid conditions. At the end of Zone I, the pollen assemblage quickly becomes dominated by *Picea, Pinus, Abies* and *Fagus*. This

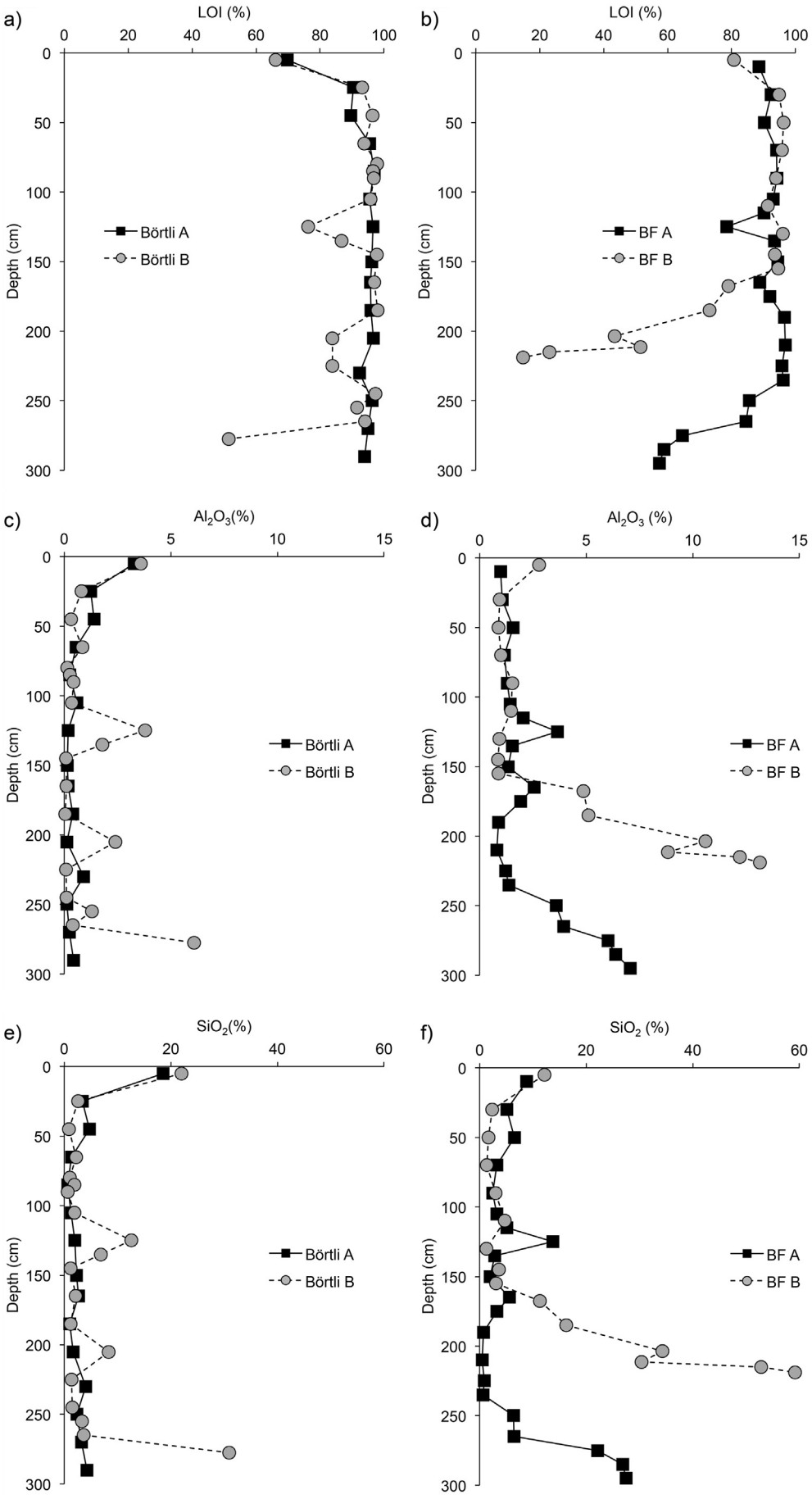

Fig. 5. Major chemical compounds along the mire profiles: LOI for the site a) Börtli and b) BF (Brätschenflue), Al_2O_3 (c: Börtli and d: BF) and SiO_2 (e: Börtli and f: BF).

Table 6
Analysed material and related results of radiocarbon dating.

Site	UZH–/ETHZ–Code	Depth	Material	$\delta^{13}C$	Uncalibrated ^{14}C age	Calibrated age (2σ)
		(cm)		(‰)	(a BP)	(cal a BP)
Börtli	UZ–6335/ETH–66271	30–40	Peat	− 25.0 ± 1.0	1745 ± 24	1714–1570
	UZ–6336/ETH–66272	85–95	Wood	− 24.9 ± 1.0	3391 ± 25	3695–3576
	UZ–6444/ETH–75850	120–130	Peat	− 30.8 ± 1.0	6659 ± 25	7580–7489
	UZ–6339/ETH–66275	160–170	Peat	− 25.3 ± 1.0	7112 ± 29	8001–7866
	UZ–6338/ETH–66274	235–245	Peat	− 28.2 ± 1.0	8084 ± 30	9121–8815
	UZ–6443/ETH–75849	290–300	Peat	− 26.6 ± 1.0	7602 ± 26	8429–8372
BF A	UZ–6330/ETH–66266	30–40	Peat	− 24.2 ± 1.0	427 ± 23	520–463
	UZ–6331/ETH–66267	100–110	Peat	− 26.3 ± 1.0	1624 ± 24	1568–1415
	UZ–6332/ETH–66268	150–160	Peat	− 26.3 ± 1.0	3071 ± 25	3359–3215
	UZ–6445/ETH–75851	200–210	Peat	− 23.3 ± 1.0	4353 ± 23	4972–4855
	UZ–6333/ETH–66269	250–260	Peat	− 26.6 ± 1.0	6086 ± 28	7149–6859
	UZ–6334/ETH–66270	290–300	Peat	− 28.1 ± 1.0	7731 ± 30	8581–8434
BF B	UZ–6384/ETH–69488	70–80	Peat	− 24.5 ± 1.0	1910 ± 27	1929–1743
	UZ–6385/ETH–69489	172–185	Peat	− 22.4 ± 1.0	4594 ± 29	5448–5083
	UZ–6425/ETH–73267	290–300	Peat	− 36.3 ± 1.0	7599 ± 30	8440–8364

rapid change in individual species strongly suggests the presence of a hiatus and a phase of cooling climate.

- Phase II (170–110 cm; 3.6 to 1.9 cal ka BP) was marked by a further increase in *Pinus* (up to 50%), *Picea* (30%), *Alnus* (10–25%), *Abies* (5–7%) and *Fagus* (3–4%). In addition, the proportion of Cyperacea continuously increased during this period. This phase would correspond with the Löbben and Göschener cold phase I (Ivy-Ochs et al., 2009).
- Phase III (110–70 cm; 1.9–1.0 cal ka BP) starts with as strong decrease of *Pinus* (from 50% to 20%), accompanied by a decrease of *Alnus* and *Picea*. These fluctuations correlate with the appearance of *Populus* (2.6%) and an increase in Cyperaceae and Poaceae. The presence of *Populus* may reflect either environmental change or human impact as it is a species that is well adapted to fire.
- Phase IV (70–0 cm; the last thousand years) is dominated by *Pinus* (30–50%), *Picea* (20%) and Alnus (10–15%). Human impact is now more evident with a high proportion of NAP and the appearance of human activity-related species such as Cerealia, Calluna, Rumex, Rannunculaceae, Galium, Plantago, Brassicacea and Cypaeraceae.

4. Discussion

4.1. Glacier dynamics close to the onset of the Holocene

The ^{14}C–dates at the base of the peat bogs support the relative stratigraphy and chronological sequence inferred by the ^{10}Be dates. The integrated ages indicate that organic material must have started to accumulate in the mires at the latest about 1000–2000 years after the ice retreat. The time gap between morainic deposition and subsequent organic sedimentation inside the former forefield area cannot be fully explained at the moment, but this is a common uncertainty in ^{14}C analyses of bog-bottom organics in alpine regions worldwide (e.g,Madole, 1976; Maisch, 1982). It certainly took time for vegetation to be established and for sedimentation to begin before mires could develop here.

Together, surface exposure ages from moraine boulders and the radiocarbon ages from the peat bog bases indicate that during the Younger Dryas the whole Göschenertal was under ice (Fig. 3). Subsequent warming led to a vanishing of the glaciers. Renner (1982) tried to correlate the corresponding glacial stadial in the Göschener valley with the stadial of the nearby Urseren-valley by using the regional morphostratigraphy of Central Switzerland. This stadial was attributed to the Daun Stadial of the Eastern Alps (Renner, 1982) which in turn was assigned a Pre-Bølling age (> 14.7 ka BP). Our evidence suggests that that this age was too old.

4.2. Soils

The weathering indices of the soil profiles show that soils are polygenetic with complex evolution histories. The lithological discontinuities within the profiles indicate these were affected by both erosion and accumulation. This is not surprising because the soils are located on steep slopes in a high-alpine region. The upper horizons of the soils (Ah1-Ah2) reflect a younger, less weathered material. The

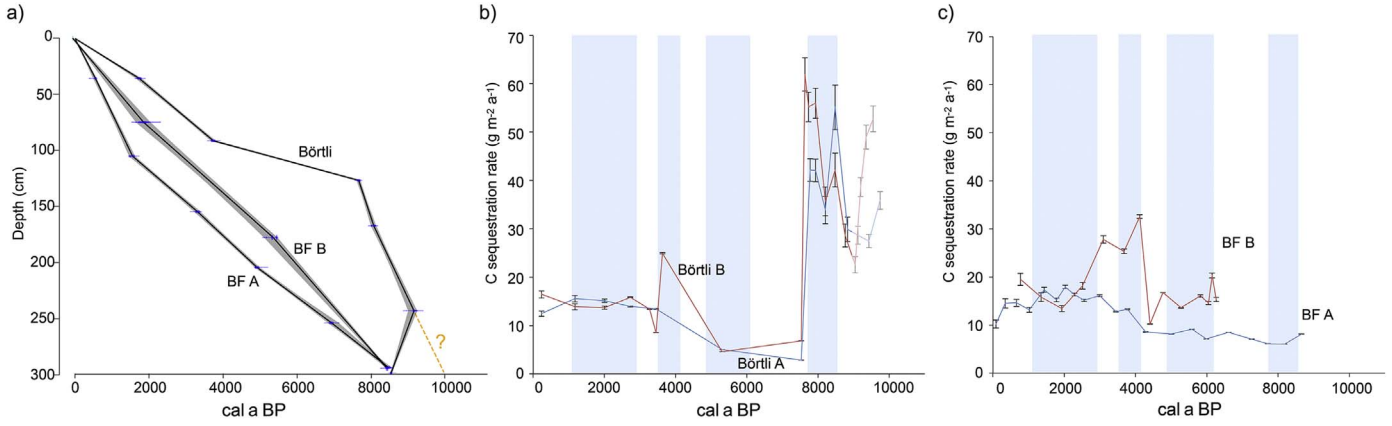

Fig. 6. a) Age-depth model of the investigated cores and carbon sequestration rates over time for the site b) Börtli and c) BF. The semi-transparent lines in b) indicate the extrapolated trend before 9 ka BP.

Fig. 7. Pollen spectra along the cores Börtli A and BF A (Brätschenflue).

lower profiles (2Bsb horizons) with their reddish hues and high chroma-values (Table 3) testify a relatively long and intense weathering period. This period was later interrupted by erosion, after which accumulation processes (or soil creep) began again. During the evolution of the soils, progressive and regressive phases must have occurred. Soils may respond clearly and diversely to climate change and human impact (Brisset et al., 2013; Egli and Poulenard, 2017). To explain the details of soil dynamics over time is, however, a very challenging task (Egli and Poulenard, 2017). An increased disequilibrium with climate may induce rapid changes to soils, but quantitative data are mostly missing. Overall changes in precipitation patterns, temperature regime and snow cover will distinctly influence mountain vegetation and thus also soils. Studies of (palaeo)soils, soil charcoal or lacustrine sedimentary archives (Mourier et al., 2010) have confirmed the succession of progressive — e.g., during the first part of the Holocene (before the 8.2 ka BP event) and also during the Mid-Holocene (Veit, 1993; Brisset et al., 2013) — and regressive phases of soil genesis in these mountain areas. Temporal sequences developed only through soil analyses is very difficult and in our case impossible without considering nearby archives. A similar approach was chosen by Tinner et al. (1996) who showed that climatic conditions in the Swiss Alps varied considerably between 9.5 and 4.6 ka BP which affected vegetation and seemingly also soil development.

4.3. Mires: mirror of soil and landscape processes

The Brätschenflue mires started to accumulate peat near the transition from the Boreal to the Older Atlantic chronozone. Based on its geomorphic position, the Börtli mire is older; although definitive proof is lacking, it seems to have developed since the end of the Preboreal chronozone. A ^{14}C–age inversion at the transition of the mire to the basal sediment makes it impossible to precisely date when ice retreated from its location. Because of this inverted age, we extrapolated a linear age model in order to cover the full range of the analysed proxy (Falkiewicz-Koziel et al., 2014).

We calculated sequestration rates of organic carbon over time based on our (above) age-depth model. This approach is, however, subject to limitations (see below). It nonetheless seems that carbon sequestration rates and thus peat formation was enhanced during cooler periods such as the Göschener I and II cold phases (roughly about 800 years within 1–3 ka BP; Zoller, 1966), the climatic shift (cold phase) near 4.2 ka BP, the Piora cold phases (5–6 ka BP; only Brätschenflue) and particularly during the 8.2 ka BP Misox cold phases (Magny, 2004; Savi et al., 2014). The cooler conditions seem to inhibit organic matter decay, giving rise to a net accumulation. The sequestration rates were similar in both mires (varying between 4 and 62 g C m^{-2} a^{-1}). The average C sequestration rate over all sites and time was 21.1 g C m^{-2} a^{-1} (long-term apparent rates of C accumulation - LARCA). The LARCA is a common method of assessing long-term peat accumulation (Clymo et al., 1998); it calculates the rate of C accumulation by dividing the mass of C per unit area by the age of the peatland. The method is simple, but must be used with care, because it calculates only the apparent rate of C accumulation and does not account for decay after the peat was formed. Because of this limitation, caution must be used when comparing the LARCA values of peatlands of different ages (Hribljan et al., 2015). Hribljan et al. (2015) measured a LARCA value of 37–47 g m^{-2} a^{-1} in high-alpine peats (Bolivian highlands). In the Ecuadorian páramo, sequestration rates are 12–50 g m^{-2} a^{-1} while in North American mountain peatlands the average measured values are 25 g m^{-2} a^{-1} (Chimner, 2000; Chimner and Karberg, 2008; Hribljan et al., 2015). The measured values for the Göscheneralp (4–62 g C m^{-2} a^{-1}) lie in the range of these worldwide sequestration rates.

During almost all cold phases of the Holocene, the mires at Börtli and Brätschenflue seem to have received a higher sediment input relative to the warm phases (Fig. 8). The geochemical and mineralogical composition of the peat and the association of chemical elements are consistent with the character of the local geology. Consequently, the sediment input is obviously due to erosion from surrounding landscapes. The geochemistry of the sediment input exhibits lower weathering values than the inorganic part of the peat in between these periods. Those chemical ratios (Ti/Zr, K/Rb; Fig. 9) that are commonly applied to determine changes in lithogenic sources, varied distinctly along the profiles (Silva-Sánchez et al., 2015). The Ti/Zr, K/Rb ratios of the Börtli mire profile followed similar trends to those observed for the inorganic components (Al_2O_3, SiO_2 or weathering indices). The Ti/Zr, K/Rb ratios are less clear for BF A; particularly for the last 4 ka, strong variations were measured. It seems that weakly- to moderately-weathered soil particles were washed into the Börtli site during erosion events. During stable phases, either more strongly weathered particles were occasionally transferred into the mires or there was a larger aeolian flux, as indicated by the (Ca + K)/Ti, Ti/Zr or K/Rb ratios.

To study such possible aeolian additions to the soils, it is helpful to use chemically immobile elements (Dahms and Egli, 2016). We chose the elements Ti, Zr, Nb, Ce, and Y, all of which have a relatively high ionic potential and are considered to be chemically immobile under most near-surface environments (Hutton, 1977; Taylor and McLennan, 1985; Muhs and Benedict, 2006). According to Muhs and Benedict (2006), Tb and Nb are found in ilmenite, rutile, anatase, titanomagnetite, sphene, and biotite. Zr is mostly present in zircon, although Zr may also be found in other minerals (e.g. zirconolite). The rare earth elements (REE) Ce and Y are related to a wide variety of minerals such as phyllosilicates (adsorption on e.g., micas, chlorite, other clay minerals), sphene, amphiboles and apatite (Muhs and Benedict, 2006). Fig. 10 demonstrates that a considerable part of the chemical signature (Ti/Zr vs Ti/Nb) of Börtli A and B are close to the soils' signature. A large part of BF A and BF B do not match the soils' signature and a considerable part of the chemical imprint of the Brätschenflue mire seems to indicate aeolian input. If the Ti/Zr-ratios are compared with the Ce/Y ratios (Fig. 10), then large parts of the chemical signatures of the mires are outside the range we measured in the soils.

Although not all mires react in the same way, a general soil redistribution pattern can nonetheless be depicted. It seems that during almost all known cooler phases during the Holocene, soil erosion was more intense and less weathered material was transferred into the mires. Many of these erosion events have a natural character because human impact does not seem to appear until about 2 ka BP. Human impact distinctly increased between about 2 ka BP and today; this is clearly reflected in the pollen composition of the mires (import of new species that are related to anthropogenic activity). A higher human impact is recorded since about 3 ka BP also in other parts of the Alps. First signs of human activity can often be detected about 3–5 ka BP (Tinner et al., 1996; Schmidt et al., 2002; Wick et al., 2003; Giguet-Covex et al., 2011; Brisset et al., 2013; Jäger et al., 2015) and in some cases even earlier (Schwörer et al., 2014).

Mourier et al. (2010) and other authors (e.g., Schwörer et al., 2014) report favourable conditions for pedogenesis after deglaciation until ca. 8.4 ka BP. Thereafter we see evidence of strong erosion processes in the soils. This phenomenon not only appears in the European Alps but also in other similar alpine regions such as the Karkonosze Mountains in Poland and Czechia (Engel et al., 2010; Malkiewitz et al., 2016). During this period, the climate in western and central Europe was characterised by cooler and wetter conditions and a marked climatic irregularity in the northern Mediterranean basin (Berger and Guilaine, 2009). The cooling phase is documented in pollen spectra and in speleothem records throughout the northern hemisphere and by $\delta^{18}O$ data from Greenland ice cores that shows a decrease in temperature of around 7 °C in less than a decade (Alley and Augustdottir, 2005). A sandy layer and the chemical imprint (e.g. Al-content, Fig. 8) in the Börtli mire indicates the presence of a strong erosive phase associated with regressive pedogenesis in the soil profiles on the slope above the mire. This major cooling phase obviously also affected vegetation — in our

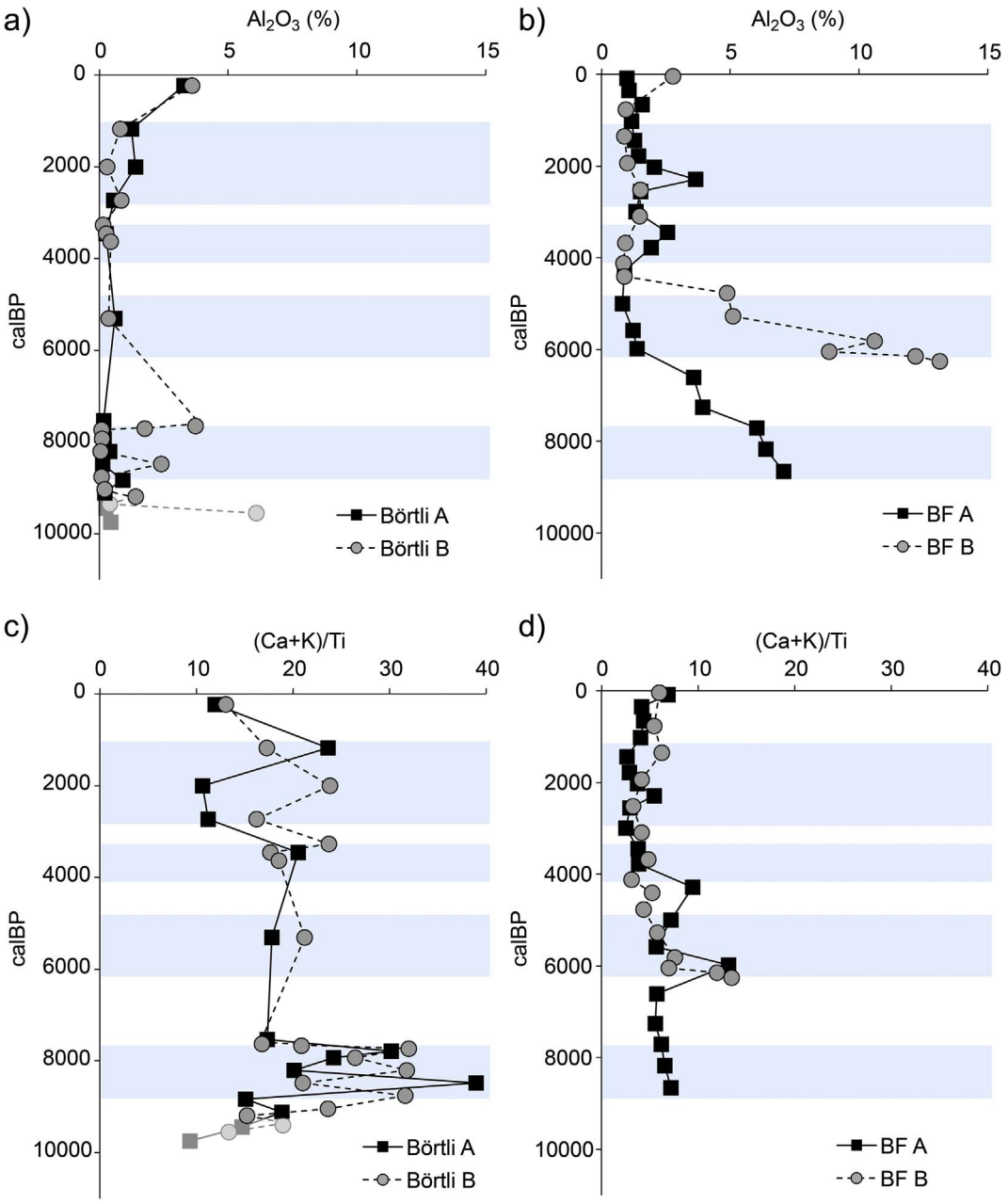

Fig. 8. Al_2O_3 concentrations (as an indicator of detritus input) along the profiles (given as age) a) Börtli A and B and b) BF (Brätschenflue) A and B. The weathering index (Ca + K)/Ti is given for c) the Börtli cores and d) the BF cores. The semi-transparent points in a) and c) indicate the extrapolated trend before 9 ka BP.

case with a low AP:NAP ratio. In literature, this cold phase was not recognised in all investigated lake and mire archives. Evidence, due to a change in vegetation, was found in the northwestern Swiss Alps (Schwörer et al., 2014). In other parts of the French Alps, however, no clear sign of a cold phase was found (Giguet-Covex et al., 2011). In the Austrian Alps, the low pollen productivity indicated that a cold phase had affected vegetation (Kofler et al., 2005).

In some parts of the Alps, a higher rate of erosion seems to have occurred about 6.5–7.2 ka BP. This can be related, in part, to a change in forest fire regimes associated with human impact (Mourier et al., 2010). Tinner et al. (1996) report that a strong climatic deterioration caused an opening of timberline forest. Such a phase is, however, not evident in our data from the Göschenertal. An expansion of forests and a reduced erosion rates after 6.3 ka BP seem to have occurred in several parts of the Alps (Lotter and Birks, 2003; Wick et al., 2003; Schwörer et al., 2014).

Another distinct erosional phase occurred ca. 5–6 ka BP that fits to the Piora cold phase (Ivy-Ochs et al., 2009). Similar to our case, higher rates of erosion and sedimentation were recorded in the Karkonosze mountains at this time (Engel et al., 2010; 5.8–5.5 cal ka BP) and also other parts of the Alps (Schmidt et al., 2002). The cold phase about 5–6 ka BP also affected the vegetation distribution. The proportion of *Betula* and *Pinus* strongly decreased and the share of *Alnus* and *Picea* increased. An additional cold event is known to have occurred around 4.2 ka BP (Engel 2010; Brisset et al., 2013). An abrupt cool-climate pulse and/or rapid environmental changes have been identified around 4.2 ka BP in the Northern Hemisphere (Booth et al., 2005; Huang et al., 2011; Magny et al., 2009; Brisset et al., 2013) and regionally in the northern part of the Mediterranean basin (Drysdale et al., 2006; Miramont et al., 2008). According to Brisset et al. (2013), this cooling phase was accompanied by major detrital pulses in regions undergoing increased human pressure. This change is also seen in our Göschener-

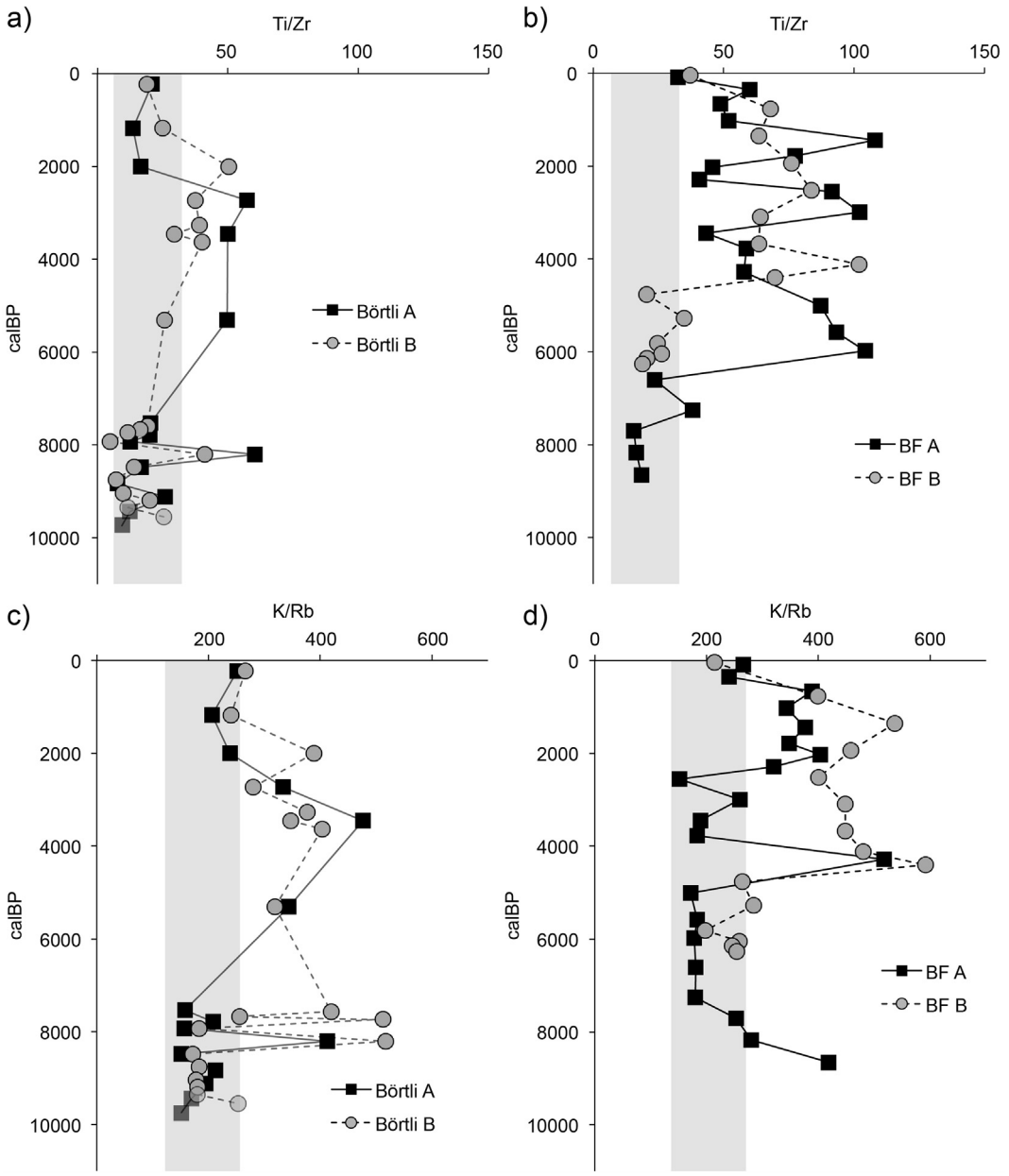

Fig. 9. Chemical ratios of a + b) Ti/Zr and c + d) K/Rb in the mires (Börtli A and B; BF (Brätschenflue) A and BF B) as a function of age. The grey area indicates the range that was measured in the soils. The semi-transparent points in a) and c) indicate the extrapolated trend before 9 ka BP.

valley mires as a slight increase in erosion activity (mire BF A).

According to Zoller (1966), the Göschener cold phases (I and II) seem to have occurred between 1 and 3 ka BP. These cold phases increasingly overlap with human activity in the study area. The effect of this potential cooling phase is therefore difficult to distinguish from human impact. The Börtli A and the BF A mires showed that more erosion occurred during this time span, an observation that was also noted by Favilli et al. (2009) in the Italian or by Veit (1993) in Austria and the southern Tyrolean Dolomites. Except for BF A, all the Göschenen valley mires show evidence of more erosion during the last 1000 years. This development is probably due more to the effects of human impacts than to the Little Ice Age.

More kaolinite is detected in the mire profiles after ca. 3.5–5 cal ka BP. Kaolinite can have an aeolian origin and it is known that the Alps receive every year a minor dust input from the Sahara. The chemical signal of the Brätschenflue mire also changed about 5–6 ka ago. This is shown by the increases we see in Ti/Zr and K/Rb ratios of the Göschenen valley soils at this time. Indeed, the K/Rb ratios reported for Sahara dust generally are higher than in the soils of our study area (Göschenen valley soil K/Rb in the range of 150–230; Sahara dust K/Rb in the range of 140–400; Eltayeb et al., 2001; Moreno et al., 2006). Likewise, the Ti/Zr ratio of the Göschenen valley soils is in the range of 12–32, whereas a ratio of 33–40 is reported for Sahara dust (Muhs et al., 1990). Consequently, the higher ratios of K/Rb and Ti/Zr in our soils might partially be affected by Sahara dust. Occasionally, these ratios are very high, and yet, they do not fit the reported range of values for Sahara dust. There might be other sources, but a provenance from the Sahara would make most sense here. It is also known that the climate of the Sahara was wetter during the African Humid Period (AHP) about 11 to 5.5 cal ka BP (Manning and Timpson, 2014). Dust fluxes from the Sahara abruptly changed about 5 ka ago, and have continued to increase since then (Adkins et al., 2006; McGee et al., 2013).

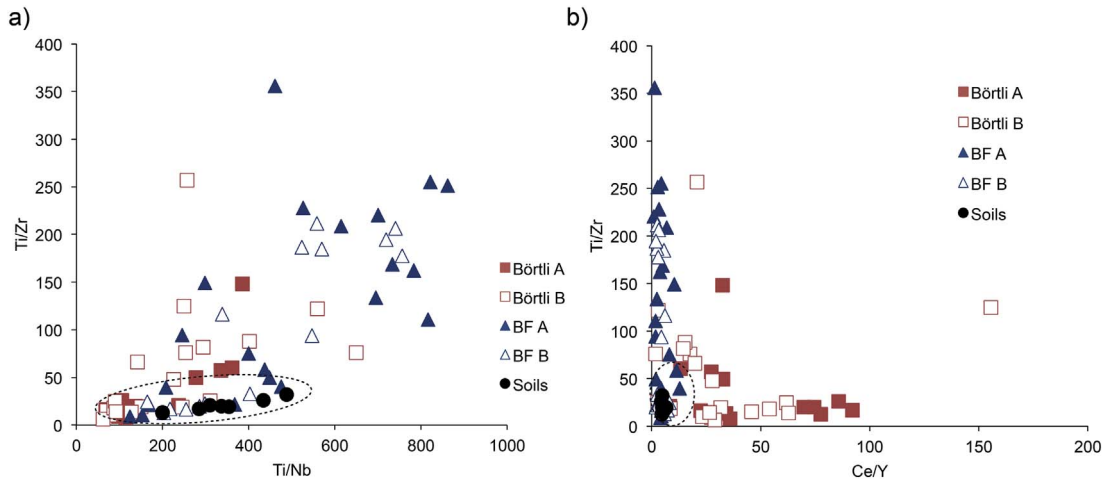

Fig. 10. Binary diagram of concentration ratios of a) Ti/Zr vs Ti/Nb and b) Ti/Zr vs Ce/Y for the mire profiles Börtli A, B and BF (Brätschenflue) A, B. In addition the values are also given for the investigated soils. The dashed lines indicate roughly the field where soil data occur.

5. Conclusions

Geochemical tracers and ^{14}C ages of mire sediments, when combined with analyses of soils on surrounding slopes enable us to decipher the details of landscape processes in the Göschenen valley of the Central Swiss Alps. Several phases with progressive and regressive soil development have occurred in the Central Alps and can be correlated to the Holocene cold and warm phases that we geochemically recognise in our alpine mires. By using this geochemical forensic approach, we find that climate cooling (often coupled with a higher precipitation) seems to have intensified soil mass redistribution here. In addition, we also find that, as hypothesised, carbon sequestration rates in the mires were higher during the cold phases.

After deglaciation, that was dated to the end of the Younger Dryas in the Göschener valley, soil evolution was probably dominated by progressive development until about 8 ka BP. Although not all mires showed a similar pattern, higher geomorphic dynamics and soil redistribution seem to have occurred particularly around 8 ka BP. Other phases of environmental change occurred ca. 5–6 ka, 4 ka, and 1–3 ka BP. The cooling phase about 8 ka ago led to a distinct change in the vegetation distribution (tendency towards increasing tundra) and erosion rates seem to have been particularly pronounced during this period. The cold phase at 5–6 ka BP also had an effect on the vegetation, but less distinctly. With respect to phases of erosion and regressive soil formation at this time, the effects seem to have been minimal and the carbon accumulation rates remained nearly static.

Human impact is increasingly detectable after ca. 2.4 ka BP from the appearance of new plant species here. The appearance of these new species overlaps the potential 'Göschener cold phase'. During this period, rates of C accumulation and erosion increased slightly. We observe an increase in the rate of erosion over the last 1 ka that seems to be connected to anthropogenic activity.

Aeolian input has become increasingly important for the last 5 ka. This pattern seems to be concurrent with the climate and landscape changes observed for the Sahara over this period. Although several phases can be distinguished with higher rates of erosion, soil evolution evidently was not completely regressive during such phases; but the processes leading to regressive soil evolution became more frequent, particularly on slopes close to or above timberline.

Acknowledgements

This research was supported by the Swiss Government Excellence Scholarship (2016.0646/Brazil/OP) for Raquel de Castro Portes. We would like to thank Stefan Gamma (Wasserwelten Göschenen), Felix Renner and Kseniia Ashastina for their interest in our project and support in the field. We are, furthermore, indebted to Susan Ivy-Ochs for fruitful discussions and to two unknown reviewers for their helpful comments on an earlier version of the manuscript.

References

Adkins, J., deMenocal, P., Eshel, G., 2006. The "African humid period" and the record of marine upwelling from excess ^{230}Th in Ocean Drilling Program Hole 658C. Paleoceanography 21, PA4203. http://dx.doi.org/10.1029/2005PA001200.

Alley, R., Augustdottir, A.M., 2005. The 8k event: cause and consequences of a major Holocene abrupt climate change. Quat. Sci. Rev. 24, 1123–1149.

Bennett, K.D., Willis, K.J., 2002. Pollen. In: Smol, J.P., Birks, H.J.B., Last, W.M. (Eds.), Tracking Environmental Change Using Lake Sediments. Volume 3: Terrestrial, Algal, and Siliceous Indicators. Kluwer Academic Publishers, New York, Boston, Dordrecht, pp. 5–32.

Berger, J.F., Guilaine, J., 2009. The 8200 cal BP abrupt environmental change and the Neolithic transition: a Mediterranean perspective. Quat. Int. 200, 31–49.

Birks, H.H., 2002. Plant macrofossils. In: Smol, J.P., Birks, H.J.B., Last, W.M. (Eds.), Tracking Environmental Change Using Lake Sediments. Volume 3: Terrestrial, Algal, and Siliceous Indicators. Kluwer Academic Publishers, New York, Boston, Dordrecht, pp. 49–74.

Blaauw, M., 2010. Methods and code for 'classical' age-modelling of radiocarbon sequences. Quat. Geochronol. 5, 512–518.

Blockley, S.P.E., Lane, S.C.S., Hardiman, M., Rasmussen, S.O., Seierstad, I.K., Steffenson, J.P., Svensson, A., Lotter, A.F., Turney, C.S.M., Bronk Ramsey, C., INITMATE members, 2012. Synchronisation of palaeoenvironmental records over the last 60,000 years, and an extended INTIMATE event stratigraphy to 48,000 b2k. Quat. Sci. Rev. 36, 2–10.

Booth, R.K., Jackson, S.T., Forman, S.L., Kutzbach, J.E., Bettis, I., E.A., Kreig, J., Wright, D.K., 2005. A severe centennial-scale drought in midcontinental North America 4200 years ago and apparent global linkages. The Holocene 15, 321–328.

Borchers, B., Marrero, S., Balco, G., Caffee, M., Goehring, B., Lifton, N., Nishiizumi, K., Phillips, F., Schaefer, J., Stone, J., 2016. Geological calibration of spallation production rates in the CRONUS-earth. Quat. Geochronol. 31, 188–198.

Brisset, E., Miramont, C., Guiter, F., Anthony, E., Tachikawa, K., Poulenard, J., Arnaud, F., Delhon, F., Meunier, J.-D., Bard, E., Sumera, F., 2013. Non-reversible geosystem destabilisation at 4200 cal. BP: sedimentological, geochemical and botanical markers of soil erosion recorded in a Mediterranean Alpine Lake. The Holocene 23, 1863–1874.

Bronk Ramsey, C., 2001. Development of the radiocarbon calibration program. Radiocarbon 43, 355–363.

Bronk Ramsey, C., 2009. Bayesian analysis of radiocarbon dates. Radiocarbon 51, 337–360.

Brown, E.T., Edmond, J.M., Raisbeck, G.M., Yiou, F., Desgarceaux, S., 1992. Effective attenuation length of cosmic rays producing ^{10}Be and ^{26}Al in quartz: implications for surface exposure dating. Geophys. Res. Lett. 9, 369–372.

Buggle, B., Glaser, B., Hambach, U., Gerasimenko, N., Markovic, S., 2011. An evaluation of geochemical weathering indices in loess-paleosol studies. Quat. Int. 240, 12–21.

Burga, C.A., Perret, R., 1998. Vegetation und Klima der Schweiz seit dem jüngeren Eiszeitalter. Ott Verlag, Thun.

Chmeleff, J., von Blanckenburg, F., Kossert, K., Jakob, D., 2010. Determination of the ^{10}Be half-life by multicollector ICP-MS and liquid scintillation counting. Nucl. Instrum. Methods Phys. Res. Sect. B 268, 192–199.

Christl, M., Vockenhuber, P.W., Kubik, P.W., Wacker, L., Lachner, J., Alfimov, V., Synal, H.-A., 2013. The ETH Zurich AMS facilities: performance parameters and reference materials. Nucl. Inst. Methods Phys. Res. B 294, 29–38.

Chimner, R.A., Karberg, J.M., 2008. Long-term carbon accumulation in two tropical mountain peatlands, Andes Mountains, Ecuador. Mires Peat 3, 1–10.
Chimner, R.A., 2000. Carbon Dynamics of Southern Rocky Mountain Fens. (PhD dissertation) Colorado State University, Fort Collins, CO (150 pp).
Clymo, R.S., Turunen, J., Tolonen, K., 1998. Carbon accumulation in peatland. Oikos 81, 368–388.
Dahms, D., Egli, M., 2016. Carbonate and elemental accumulation rates in arid soils of mid-to-late Pleistocene outwash terraces, southeastern Wind River Range, Wyoming, USA. Chem. Geol. 446, 147–162.
Dahms, D., Favilli, F., Krebs, R., Egli, M., 2012. Soil weathering and accumulation rates of oxalate-extractable phases from alpine chronosequences of up to 1 ma in age. Geomorphology 151-152, 99–113.
Drysdale, R., Zanchetta, G., Hellstrom, J., Maas, R., Fallik, A., Pickett, M., Cartwright, I., Piccini, L., 2006. Late Holocene drought responsible for the collapse of Old World civilizations is recorded in an Italian cave flowstone. Geology 34, 101–104.
Egli, M., Merkli, C., Sartori, G., Mirabella, A., Plötze, M., 2008. Weathering, mineralogical evolution and soil organic matter along a Holocene soil toposequence developed on carbonate-rich materials. Geomorphology 97, 675–696.
Egli, M., Maisch, M., Purves, R., Çöltekin, A., Hilbich, C., 2015. Multi-methodological reconstruction of the lake level at Morgarten in the context of the history of the Swiss Confederation. The Holocene 25, 1727–1741.
Egli, M., Poulenard, J., 2017. Soils of mountainous landscapes. In: Richardson, D., Castree, N., Goodchild, M.M., Kobayashi, A., Liu, W., Marston, R.A. (Eds.), The International Encyclopedia of Geography. John Wiley & Sons, Ltd.. http://dx.doi.org/10.1002/9781118786352.wbieg0197.
Eltayeb, M.A.H., Injuk, J., Maenhau, W., van Grieken, R., 2001. Elemental composition of mineral aerosol generated from Sudan Sahara sand. J. Atmos. Chem. 40, 247–273.
Engel, Z., Nývlt, D., Křížek, M., Treml, V., Jankovská, V., Lisá, L., 2010. Sedimentary evidence of landscape and climate history since the end of MIS 3 in the Krkonoše Mountains, Czech Republic. Quat. Sci. Rev. 29, 913–927.
Erdtman, G., 1960. The acetolysis method. Sven. Bot. Tidskr. 54, 561–564.
Faegri, K., Iversen, J., 1989. Textbook of Pollen Analysis. John Wiley, Chichester.
Farmer, V.C., Fraser, A.R., Tait, J.M., Palmieri, F., Violante, P., Nakai, M., Yoshingaga, N., 1978. Imogolite and proto-imogolite in an Italian soil developed on volcanic ash. Clay Miner. 13, 271–274.
Favilli, F., Egli, M., Brandová, D., Ivy-Ochs, S., Kubik, P.W., Cherubini, P., Mirabella, A., Sartori, G., Giaccai, D., Haeberli, W., 2009. Combined use of relative and absolute dating techniques for detecting signals of Alpine landscape evolution during the late Pleistocene and early Holocene. Geomorphology 112, 48–66.
Gamper, M., Suter, J., 1982. Postglaziale Klimageschichte der Schweiz. Geogr. Helv. 37, 105–114.
Giguet-Covex, C., Arnaud, F., Poulenard, J., Disnar, J.-R., Delhon, C., Francus, P., David, F., Enters, D., Rey, P.-J., Delannoy, J.-J., 2011. Changes in erosion patterns during the Holocene in a currently treeless subalpine catchment inferred from lake sediment geochemistry (Lake Anterne, 2063 m a.s.l., NW French Alps): the role of climate and human activities. The Holocene 21, 651–665.
Gosse, J.C., Phillips, F.M., 2001. Terrestrial in situ produced cosmogenic nuclides: theory and application. Quat. Sci. Rev. 20, 1475–1560.
Haeberli, W., Frauenfelder, R., Hoelzle, M., Maisch, M., 1999. On rates and acceleration trends of global glacier mass changes. Geogr. Ann. 81 (A), 585–591.
Heimsath, A.M., McGlynn, R., 2008. Quantifying periglacial erosion in the Nepal high Himalaya. Geomorphology 97, 5–23.
Hitz, C., Egli, M., Fitze, P., 2002. Determination of the sampling volume for representative analysis of alpine soils. Z. Pflanzenernähr. Bodenkd. 165, 326–331.
Holzhauser, H., Magny, M., Zumbuühl, H.J., 2005. Glacier and lake-level variations in west-central Europe over the last 3500 years. The Holocene 15, 789–801.
Hribljan, J.A., Cooper, D.J., Sueltenfuss, J., Wolf, E.C., Heckman, K.A., Lilleskov, E.A., Chimner, R.A., 2015. Carbon storage and long-term rate of accumulation in high-altitude Andean peatlands of Bolivia. Mires Peat 15, 1–14.
Huang, C.C., Pang, J., Zha, X., Su, H., Jia, Y., 2011. Extraordinary floods related to the climatic event at 4200 a BP on the Qishuihe River, middle reaches of the Yellow River, China. Quat. Sci. Rev. 30, 460–468.
Hutton, J.T., 1977. Titaniumand zirconium minerals. In: Dixon, J.B., Weed, S.B. (Eds.), Minerals in Soil Environments. Soil Science Society of America, Madison, Wisconsin, pp. 673–688.
IUSS Working Group WRB, 2015. World Reference Base for Soil Resources 2014, Update 2015. International Soil Classification System for Naming Soils and Creating Legends for Soil Maps. World Soil Resources Reports. 106 FAO, Rome.
Ivy-Ochs, S., 1996. The Dating of Rock Surfaces Using In Situ Produced ^{10}Be, ^{26}Al and ^{36}Cl, with Examples from Antarctica and the Swiss Alps. (PhD Thesis, ETH Zurich, No. 11763).
Ivy-Ochs, S., Kerschner, H., Reuther, A., Maisch, M., Sailer, R., Schaefer, J., Kubik, P.W., Synal, H.-A., Schlüchter, C., 2006. The timing of glacier advances in the northern European alps based on surface exposure dating with cosmogenic ^{10}Be, ^{26}Al, ^{36}Cl, and ^{21}Ne. Geol. Soc. Am. Spec. Pap. 415, 43–60.
Ivy-Ochs, S., Kerschner, H., Maisch, M., Christl, M., Kubik, P.W., Schlüchter, C., 2009. Latest Pleistocene and Holocene glacier variations in the European Alps. Quat. Sci. Rev. 28, 2137–2149.
Jäger, H., Achermann, M., Waroszewski, J., Kabala, C., Malgorzata, M., Gärtner, H., Dahms, D., Krebs, R., Egli, M., 2015. Mire sediments as a mirror of erosion and soil formation. Catena 128, 63–79.
Joerin, U.E., Stocker, T.F., Schlüchter, C., 2006. Multicentury glacier fluctuations in the Swiss Alps during the Holocene. The Holocene 16, 697–704.
Joerin, U.E., Nicolussi, K., Fischer, A., Stocker, T.F., Schlücter, C., 2008. Holocene optimum events inferred from the subglacial sediments at Tschierva Glacier, Eastern Swiss Alps. Quat. Sci. Rev. 27, 337–350.
Johnson, D.L., Watson-Stegner, D., 1987. Evolution model of pedogenesis. Soil Sci. 143, 349–366.
Kofler, W., Krapf, V., Oberhuber, W., Bortenschlager, S., 2005. Vegetation responses to the 8200 cal. BP cold event and to long-term climatic changes in the Eastern Alps: possible influence of solar activity and north atlantic freshwater pulses. The Holocene 15, 779–788.
Kohl, C.P., Nishiizumi, K., 1992. Chemical isolation of quartz for measurement of in-situ produced cosmogenic nuclides. Geochim. Cosmochim. Acta 56, 3583–3587.
Korschinek, G., Bergmaier, A., Faestermann, T., Gerstmann, U.C., Remmert, A., 2010. A new value for the half-life of ^{10}Be by heavy-ion elastic recoil detection and liquid scintillation counting. Nucl. Instrum. Methods Phys. Res. Sect. B 268, 187–191.
Kronberg, G.I., Nesbitt, H.W., 1981. Quantification of weathering of soil chemistry and soil fertility. J. Soil Sci. 32, 453–459.
Kubik, P.W., Christl, M., 2010. ^{10}Be and ^{26}Al measurements at the Zurich 6 MV tandem AMS facility. Nucl. Instrum. Methods Phys. Res. Sect. B 268, 880–883.
Labhart, T.P., 1992. Geologie der Schweiz. Ott Verlag, Thun.
Lotter, A., Birks, H., 2003. Holocene sediments of Sägistalsee, a small lake at the present-day tree-line in the Swiss Alps. J. Paleolimnol. 30, 253–260.
Madole, R.F., 1976. Bog stratigraphy, radiocarbon dates, and Pinedale to Holocene glacial history in the front range, Colorado. J. Res. U. S. Geol. Surv. 4 (2), 163–169.
Magny, M., Vannière, B., Zanchetta, G., Fouache, E., Touchais, G., 2009. Possible complexity of the climatic event around 4300–3800 cal. BP in the central and western Mediterranean. The Holocene 19, 823–833.
Magny, M., 2004. Holocene climate variability as reflected by mid-European lake-level fluctuations and its probable impact on prehistoric human settlements. Quat. Int. 113, 65–79.
Maisch, M., 1982. Zur Gletscher- und Klimageschichte des alpinen Spätglazials. Geogr. Helv. 37, 93–104.
Malkiewicz, M., Waroszewski, J., Bojko, O., Egli, M., Kabala, C., 2016. Holocene vegetation history and soil development reflected in the lake sediments of the Karkonosze Mountains (Poland). The Holocene 26, 890–905.
Masarik, J., Frank, M., Schaefer, J.M., Wieler, R., 2001. Correction of in-situ cosmogenic nuclide production rates for geomagnetic field intensity variations during the past 800,000 years. Geochim. Cosmochim. Acta 65, 2995–3003.
Masarik, L., Wieler, R., 2003. Production rates of cosmogenic nuclides in boulders. Earth Planet. Sci. Lett. 216, 201–208.
Mavris, C., Furrer, G., Dahms, D., Anderson, S., Blum, A., Goetze, J., Wells, A., Egli, M., 2015. Decoding potential effects of climate and vegetation change on mineral weathering in alpine soils: an experimental study in the Wind River Range (Wyoming, USA). Geoderma 255-256, 12–26.
McGee, D., deMenocal, P.B., Winckler, G., Stuut, J.B.W., Bradtmiller, L.I., 2013. The magnitude, timing and abruptness of changes in North African dust deposition over the last 20,000 yr. Earth Planet. Sci. Lett. 371–372, 163–176.
Miramont, C., Boutterin, C., Sivan, O., Bruneton, H., Mantran, M., 2008. Grandes séquences et principales ruptures morphogéniques en Haute Provence – les complexes sédimentaires des petits organismes torrentiels de moyenne Durance. Cahiers Paléoenviron. 6, 145–154.
Moreno, T., Querol, X., Castillo, S., Alastuey, A., Cuevas, E., Herrmann, L., Mounkalila, M., Elvira, J., Gibbons, W., 2006. Geochemical variations in aeolian mineral particles from the Sahara-Sahel Dust Corridor. Chemosphere 65, 261–270.
Mourier, B., Poulenard, J., Chauvel, C., Faivre, P., Carcaillet, C., 2008. Distinguishing subalpine soil types using extractible Al and Fe fractions and REE geochemistry. Geoderma 145, 107–120.
Mourier, B., Poulenard, J., Carcaillet, C., Williamson, D., 2010. Soil evolution and subalpine ecosystem changes in the French Alps inferred from geochemical analysis of lacustrine sediments. J. Paleolimnol. 44, 571–587.
Muhs, D.R., Benedict, J.B., 2006. Eolian additions to late Quaternary alpine soils, Indian Peaks Wilderness Area, Colorado Front Range. Arct. Antarct. Alp. Res. 38, 120–130.
Muhs, D.R., Bush, C.A., Stewart, K.C., Rowland, T.R., Crittenden, R.C., 1990. Geochemical evidence of Saharan dust parent material for soils developed on Quaternary limestones of Caribbean and Western Atlantic Islands. Quat. Res. 33, 157–177.
Nalepka, D., Walanus, A., 2003. Data processing in pollen analysis. Acta Palaeobot. 43, 125–134.
Nicolussi, K., Kaufmann, M., Patzelt, G., van der Plicht, J., Thurner, A., 2005. Holocene tree-line variability in the Kauner Valley, Central Eastern Alps, indicated by dendrochronological analysis of living trees and subfossil logs. Veg. Hist. Archaeobotany 14, 221–234.
Nishiizumi, K., Imamura, M., Caffee, M.W., Southon, J.R., Finkel, R.C., McAninch, J., 2007. Absolute calibration of ^{10}Be AMS standards. Nucl. Instrum. Methods Phys. Res. Sect. B 258, 403–413.
Parker, A., 1970. An index for weathering for silicate rocks. Geol. Mag. 107, 29–147.
Pigati, J.S., Lifton, N.A., 2004. Geomagnetic effects on time-integrated cosmogenic nuclide production with emphasis on in situ ^{14}C and ^{10}Be. Earth Planet. Sci. Lett. 226, 193–205.
Rasmussen, S.O., Bigler, M., Blockley, S.P., Blunier, T., Buchardt, S.L., Clausen, H.B., Cvijanovic, I., Dahl-Jensen, D., Johnsen, S.J., Fischer, H., Gkinis, V., Guillevic, M., Hoek, W.Z., Lowe, J.L., Pedro, J.B., Popp, T., Seierstad, I.K., Steffensen, J.P., Svensson, A.M., Vallelonga, P., Vinther, B.M., Walker, M.J.C., Wheatley, J.J., Winstrup, M., 2014. A stratigraphic framework for abrupt climatic changes during the Last Glacial period based on three synchronized Greenland ice-core records: refining and extending the INTIMATE event stratigraphy. Quat. Sci. Rev. 106, 14–28.
Reimer, P.J., Bard, E., Bayliss, A., Beck, J.W., Blackwell, P.G., Bronk Ramsey, C., Buck, C.E., Cheng, H., Edwards, R.L., Friedrich, M., Grootes, P.M., Guilderson, T.P., Haflidason, H., Hajdas, I., Hatté, C., Heaton, T.J., Hoffmann, D.L., Hogg, A.G., Hughen, K.A., Kaiser, K.F., Kromer, B., Manning, S.W., Nui, M., Reimer, R.W., Richards, D.A., Scott, E.M., Southon, J.R., Staff, A.R.A., Turney, C., van der Plicht, J.,

2013. IntCal13 and Marine13 radiocarbon age calibration curves 0–50,000 years cal BP. Radiocarbon 55, 1869–1887.
Renner, F., 1982. Beiträge zur Gletschergeschichte des Gotthardgebietes und dendroklimatologische Analysen an fossilen Hölzern. (PhD thesis) University of Zurich.
Savi, S., Norton, K., Picotti, V., Akçar, N., Delunel, R., Brardinoni, F., Kubik, P., Schlunegger, F., 2014. Quantifying sediment supply at the end of the last glaciation: dynamic reconstruction of an alpine debris-flow fan. GSA Bull. 126, 773–790.
Schatz, A.K., Scholten, T., Kühn, P., 2015. Paleoclimate and weathering of the Tokaj (Hungary) loess-paleosol sequence. Paleogeogr. Paleoclimatol. Paleoecol. 426, 170–182.
Schmidt, R., Koinig, K.A., Thompson, R., Kamenik, C., 2002. A multi proxy core study of the last 7000 years of climate and alpine land-use impacts on an Austrian mountain lake (Unterer Landschitzsee, Niedere Tauern). Palaeogeogr. Palaeoclimatol. Palaeoecol. 187, 101–120.
Schwörer, C., Kaltenrieder, P., Glur, L., Berlinger, M., Elbert, J., Frei, S., Gilli, A., Hafner, A., Anselmetti, F., Grosjean, M., Tinner, W., 2014. Holocene climate, fire and vegetation dynamics at the treeline in the northwestern Swiss Alps. Veg. Hist. Archaeobotany 23, 479–496.
Silva-Sánchez, N., Schofield, J.E., Mighall, T.M., Cortizas, A.M., Edwards, K.J., Foster, I., 2015. Climate changes, lead pollution and soil erosion in south Greenland over the past 700 years. Quat. Res. 84, 159–173.
Sommer, M., Gerke, H.H., Deumlich, D., 2008. Modelling soil landscape genesis – a “time split” approach for hummocky agricultural landscapes. Geoderma 145, 480–493.
Stone, J.O., 2000. Air pressure and cosmogenic isotope production. J. Geophys. Res. 105/B10 (23), 753–759.
Stromsoe, N., Marx, S.K., Callow, N., McGowan, H.A., Heijnis, H., 2016. Estimates of late Holocene soil production and erosion in the Snowy Mountains, Australia. Catena 145, 68–82.
Succow, M., Joosten, H., 2001. Landschaftsökologische Moorkunde. E. Schweizerbart'sche Verlagsbuchhandlung, Stuttgart.
Taylor, S.R., McLennan, S.M., 1985. The Continental Crust: Its Composition and Evolution. Blackwell, Oxford.
Tinner, W., Ammann, B., Germann, P., 1996. Treeline fluctuations recorded for 12,500 years by soil profiles, pollen, and plant maxrofossils in the central Swiss Alps. Arct. Alp. Res. 28, 131–147.
van der Knaap, W.O., Lamentowicz, M., van Leeuwen, J.F.N., Hangartner, D., Leuenberger, M., Mauquoy, D., Goslar, T., Mitchell, E.A.D., Lamentowicz, Ł., Kamenik, C., 2011. A multi-proxy, high-resolution record of peatland development and its drivers during the last millennium from the subalpine Swiss Alps. Quat. Sci. Rev. 30, 3467–3480.
Veit, H., 1993. Holocene solifluction in the Austrian and southern Tyrolian Alps: dating and climatic implications. Paläoklimaforschung 11, 23–32.
von Blanckenburg, F., Belshaw, N.S., O'Nions, R.K., 1996. Separation of ^{9}Be and cosmogenic ^{10}Be from environmental materials and SIMS isotope dilution analysis. Chem. Geol. 129, 93–99.
Waroszewski, J., Egli, M., Kabala, C., Kierczak, J., Brandova, D., 2016. Mass fluxes and clay mineral formation in soils developed on slope deposits of the Kowarski Grzbiet (Karkonosze Mountains, Czech Republic/Poland). Geoderma 264B, 363–378.
Wick, L., van Leeuwen, J.F., van der Knaap, W.O., Lotter, A., 2003. Holocene vegetation development in the catchment of Sägistalsee (1935 m asl), a small lake in the Swiss Alps. J. Paleolimnol. 30, 261–272.
Zollinger, B., Alewell, C., Kneisel, C., Brandova, D., Petrillo, M., Plötze, M., Christl, M., Egli, M., 2017. Soil formation and weathering in a permafrost environment of the Swiss Alps: a multi-parameter and a non-steady-state approach. Earth Surf. Process. Landf. 42, 814–835.
Zoller, H., Schindler, C., Röthlisberger, H., 1966. Postglaziale Gletscherstände und Klimaschwankungen im Gotthardmassiv und Vorderrheingebiet. Verh. Naturforsch. Ges. Basel 77, 97–164.